



## What can hydrological modelling gain from spatially explicit parameterization and multi-gauge calibration?

Xudong Zheng<sup>1</sup>, Dengfeng Liu<sup>1\*</sup>, Hao Wang<sup>2</sup>, Chuanhui Ma<sup>1</sup>, Hui Liu<sup>2</sup>, Guanghui Ming<sup>3</sup>, Qiang Li<sup>4</sup>, Mohd Yawar Ali Khan<sup>5</sup>, Fiaz Hussain<sup>6</sup>

5 <sup>1</sup>State Key Laboratory of Water Engineering Ecology and Environment in Arid Area, School of Water Resources and Hydropower, Xi'an University of Technology, Xi'an, 710048, China

<sup>2</sup>State Key Laboratory of Water Cycle and Water Security, China Institute of Water Resources and Research, Beijing, 100038, China

10 <sup>3</sup>Key Laboratory of Water Management and Water Security for Yellow River Basin (Ministry of Water Resources), Yellow River Engineering Consulting Co., Ltd., Zhengzhou 450003, China

<sup>4</sup>State Key Laboratory of Soil and Water Conservation and Desertification Control, College of Forestry, Northwest A&F University, Yangling 712100, China

<sup>5</sup>Department of Hydrogeology, Faculty of Earth Sciences, King Abdulaziz University, Jeddah 21589, Saudi Arabia

15 <sup>6</sup>Department of Land and Water Conservation Engineering, Faculty of Agricultural Engineering and Technology, PMAS-Arid Agriculture University Rawalpindi, Rawalpindi 46300, Pakistan

*Correspondence to:* Dengfeng Liu ([liudf@xaut.edu.cn](mailto:liudf@xaut.edu.cn))



**Abstract.** Traditional hydrological modelling is facing transformative pressures from the rise of data-driven approaches and increasing demands for modelling realism. With improving data availability, enhancing the spatial representation of models while imposing stronger calibration constraints offers a promising pathway to reinvigorate the predictive capabilities of physically based distributed hydrological models. However, beyond their effects on aggregated simulated responses, the underlying mechanisms and interactions through which these approaches benefit hydrological modelling remain poorly understood. To bridge this knowledge gap, this study develops an Experiment Framework to evaluate the effect of Spatially explicit Parameterization and Multi-gauge calibration, termed EF-SPM. The framework is applied a representative nested catchment through a series of intensive comparative calibration experiments, in which multiscale parameter regionalization technique is integrated with the Variable Infiltration Capacity model.

Results indicate that, compared to simpler configurations, considering both spatially explicit parameterization with multi-gauge calibration leads to consistent improvements in streamflow simulations across all sub-basins. Controlled experiments isolating individual effects further show that spatially explicit parameterization is particularly effective in improving simulations under moderate-flow to high-flow conditions (with an 18 % improvement in  $\%Bias_{FHV_I}$ ), yet at the cost of degraded performance during low-flow periods (with  $\%Bias_{FLV}$  worsening by 8.6%). On the other hand, multi-gauge calibration markedly enhances parameter identifiability by imposing stronger constraints on spatially shared parameters. This creates a trade-off with spatially explicit parameterization, which expands the parameter set, thereby reducing identifiability and subsequently increasing equifinality. Take them together, a cross-benefit can be clearly identified in the multidimensional objective space during calibration. We found that, under uniform parameterization, continuous and convex arc-shaped Pareto fronts emerged, reflecting pronounced competition among multi-gauge objectives. This competition is substantially alleviated under spatially explicit parameterization.

This study integrates two promising directions in contemporary hydrological modelling, highlighting the importance of pursuing more expressive parameterization and stronger calibration constraints in parallel, rather than prioritizing one over the other. In doing so, it provides a steppingstone for advancing distributed hydrological modelling toward a modern Model–Data Infusion framework.



## 1 Introduction

Many fields in hydrology rely on simulation-based methods to support decision-making, assess system behaviour, and  
45 advance scientific understanding. Consequently, hydrological models present a promising avenue for accurately estimating  
states and fluxes of terrestrial water systems (Tudaji et al., 2025). By providing a quantitative and process-based  
representation of hydrological dynamics, these models—when combined with advances in measurement technologies—form  
a foundational component of emerging model-data infusion frameworks (Li et al., 2024). Our previous work, which  
promoted water budget closure by integrating multi-source data through physical-hydrological process modelling, serves as a  
50 pertinent example (Zheng et al., 2025). A recent trend in the hydrological modelling community is the growing expectation  
for hydrological models to achieve higher realism and credibility (Heuer et al., 2025). This emergence is fuelled by the  
expanding availability of Earth system data and, concurrently, by the demonstrated success of deep learning frameworks,  
encouraging advocates of physical models to further highlight their inherent advantages (Feng et al., 2022). Within this  
context, there is a general consensus that both model structures and parameters should be more explicitly characterized and  
55 constrained, as much as possible, drawing on available data and prior knowledge to reduce uncertainty (Pool et al., 2025).

Considerable attention has been directed toward these efforts, including the integration of spatially distributed prior  
information to strengthen spatial representation and facilitate parameter transferability (Luo and Shao, 2022), together with  
the incorporation of additional observations and multi-objective calibration strategies to enhance parameter identifiability  
60 (Széles et al., 2020; Mei et al., 2023; Yeste et al., 2024). The rationale behind the former approach is rooted in a prevailing  
perception within the Earth system sciences that increased spatial explicitness tends to yield more realistic simulations.  
Driven by recent advances in remote sensing and Earth observation products, a growing number of successful applications  
further highlight the substantial potential of spatially explicit approaches (Wambura et al., 2018; Fenicia and Kavetski, 2021;  
Nasta et al., 2025). A particularly illustrative example is the refinement of the melt submodule by Argentin et al. (2025),  
65 where explicitly distinguishing debris-covered from debris-free glacier areas enhanced spatial heterogeneity and led to  
notable improvements in model performance over alpine catchments. However, such enhancements in spatial  
parameterization inevitably expand the parameter space and exacerbate equifinality, which may paradoxically undermine  
model realism, as right results can arise from wrong reasons (Beven, 2024).

70 Of particular concern, the pathway poses a major challenge in estimating spatially explicit parameters and ensuring their  
transferability across scales (Sun et al., 2023). Despite distributed hydrological models have been widely developed and  
applied worldwide, the challenge remains unresolved, with many modelling studies—even recent ones—still rely on  
spatially uniform parameters derived from calibration (Yousefi Sohi et al., 2024; Shrestha et al., 2025). Addressing this  
challenge requires approaches that can systematically and explicitly resolve spatial heterogeneity while maintaining physical  
75 consistency across observational and modelling scales. Among the approaches proposed, one of the most promising



approaches is the transfer function-based regionalization technique, which links hydrological parameters to readily available soil and topographic features, providing theoretically grounded physical plausibility (Gupta et al., 2014).

Building on this idea, Samaniego et al. (2010) introduced the multiscale parameter regionalization (MPR) technique to capture the cross-scale relationships between hydrological parameters and morphological variables. Comparative modelling experiments demonstrate that the MPR framework markedly outperforms standard regionalization while maintaining parameter transferability, achieving superior performance in both streamflow simulations and the reproduction of spatial patterns. A key feature underpinning this performance is the use of scale-independent global parameters (hereafter g-parameters) to fine-tune the predefined transfer functions, thereby substantially improving their generality. Taking advantage of the model-independence and high flexibility, researchers have successfully applied the MPR framework across numerous hydrological and land surface models, including mHM (Guse et al., 2024; Kholis et al., 2025), Variable Infiltration Capacity (VIC) (Mizukami et al., 2017; Sun et al., 2024), Noah-MP (Thober et al., 2022), and Structure for Unifying Multiple Modelling Alternatives (SUMMA) modelling framework (Clark et al., 2015). Leveraging this broad applicability, MPR provides a versatile workbench for investigating the role of spatially explicit parameterizations in shaping model responses, and we intend to integrate it with the VIC model in different ways to test its robustness while contributing to the broader application of the next-generation VIC-5 (Hamman et al., 2018).

Returning to the broader aim of improving model credibility, multi-objective strategies have increasingly attracted attention as a means to strengthen calibration constraints. In essence, the calibration of hydrological model parameters is an inverse problem that is underdetermined and ill-posed in most cases, a situation that becomes particularly pronounced when dealing with complex distributed models. The resulting issue of parameter equifinality has been widely discussed and recognized by the hydrological community over the past two decades (Beven, 2001; Clark et al., 2021). This means that the interactions among parameters can offset one another, so that parameter combinations with differing physical interpretations produce similar model behaviour, generating an artificial consistency that departs from the true physical system. Adopting multiple variables as objective functions for calibration, as convincingly demonstrated by Gupta et al. (1998), constitutes a viable strategy and has gradually become a new paradigm in hydrological model calibration (Gupta et al., 2008; Brunner et al., 2021). However, this also exposes a pitfall for the unwary, whereby the incorporation of external observations can introduce systematic mismatches with model outputs, including scale and representativeness inconsistencies (e.g. differences in soil depth) (Liu et al., 2012; Chagas et al., 2024). In practice, streamflow is often used as a reliable and informative calibration target, as it integrates both surface and subsurface hydrological response over the entire basin. The presence of multi-gauge in nested catchment systems, measuring streamflow from different sub-basins, thus provides a suitable setting for multi-objective calibration of hydrological models (Liu et al., 2024). There is considerable value in evaluating the benefits of multi-gauge calibration for enhancing model realism, especially for models with spatially explicit parameters, where the nested sub-basin structure captures the hierarchical patterns of hydrological responses.



110

Prompted by pressing issues in contemporary hydrological modelling, this study aims to address three critical questions: (1) How spatially explicit parameterization, compared with spatially uniform parameterization, can enhance the realism of hydrological models while introducing additional equifinality; (2) To what extent multi-gauge calibration strategies in nested catchments can better constrain parameter identifiability; and (3) Whether cross-benefits exist between these two approaches and, if so, in what form. Here, we apply the MPR technique and its VIC-specific refinements to deploy the VIC model in a representative nested catchment consisting of five sub-basins in the upper Han River basin, China. An Experiment Framework is designed to evaluate the effect of Spatially explicit Parameterization and Multi-gauge calibration, which we termed EF-SPM. Intensive calibration experiments are then carried out within the framework, comprising cases with different parameterization and calibration configurations, with the model's realism systematically evaluated from multiple aspects. Through a combination of exploratory and comparative investigations, this work seeks to provide informed insights into both the shift from lumped to spatially explicit parameterization and the calibration practices of cutting-edge distributed hydrological models.

120

## 2 Study area and data

### 2.1 Upper Han River basin

The Han River is the largest tributary of the Yangtze River and flows through Shaanxi and Hubei provinces in China. Its main channel stretches 1,577 km, draining a basin of approximately 159,000 km<sup>2</sup>, with average annual water resources of 56.6 billion m<sup>3</sup> (Fig. 1a). More than 2,700 reservoirs have been constructed along the river, including Shiquan, Ankang, and Danjiangkou reservoirs (Zhao et al., 2021). In order to minimize the influence of anthropogenic activities, this study focuses on the Upper Han River Basin (UHRB) above Shiquan Hydrological Station (Sun et al., 2013), located between 105°59'–108°38'E and 32°20'–34°16'N (Fig. 1b).

130

The basin is characterized by a predominantly mountainous landscape, with hills, plains, and platforms comprising the remainder. Spatially, the elevation distribution defines a saddle-shaped topography that exerts a controlling influence on the river network, giving rise to a well-developed dendritic drainage pattern throughout the region. A monitoring network comprising five stations was deployed (Fig. 1b): three along the main channel (Hanzhong, Yangxian, Shiquan), and two on the headwater tributaries (Youshui, Lianghekou). This configuration establishes a well-monitored nested basin (five sub-basins, Fig. 1c), which provides the basis for this study to evaluate the impacts of spatially explicit parameterization and multi-gauge calibration on hydrological modelling. Furthermore, the UHRB experiences a subtropical monsoon climate, with annual precipitation of 800–1200 mm largely concentrated from July to September, which yields abundant runoff and rendering it highly suitable for the VIC model predicated on the Xinanjiang formula (Li et al., 2022; Lehmann et al., 2022).

140

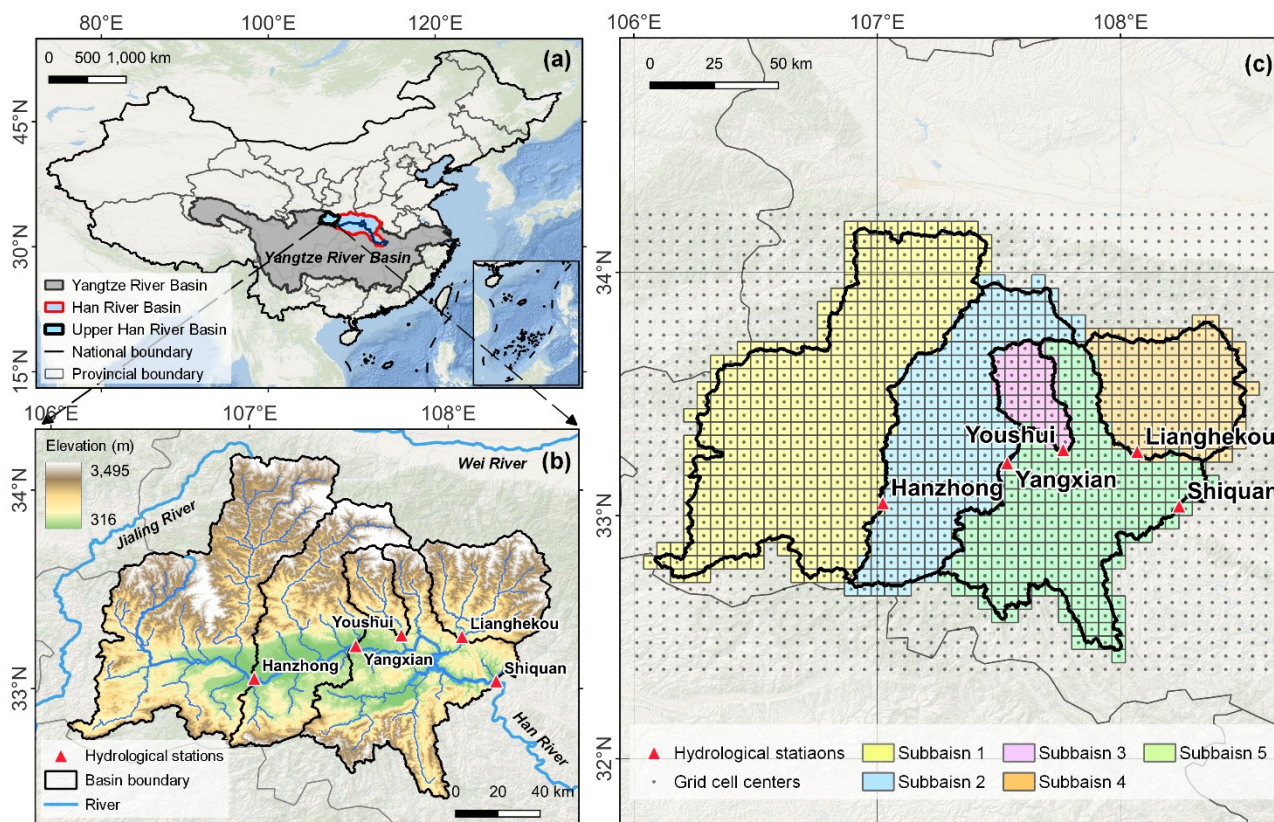


**Figure 1.** (a) Location of the Upper Han River Basin in China. (b) Elevation, hydrological stations, basin boundary, and river network. (c) Model domain discretized at  $6\text{ km} \times 6\text{ km}$  and the delineated five sub-basins. The background map is derived from the ESRI Ocean Basemap. Copyright © Esri.

## 145 2.2 Dataset

The modelling exercises of this study require a wide variety of data products, which fall into three categories: meteorological forcings, land surface characteristics, and in-situ streamflow observations. The meteorological forcings were sourced from the China Meteorological Forcing Dataset (CMFD), selected for its 3-hourly temporal resolution, which satisfies the VIC-5 image driver (hereinafter VIC-5) time-stepping scheme requirement of at least four steps per day. This dataset offers seven  
 150 key meteorological variables across China at a  $0.1^\circ \times 0.1^\circ$  spatial resolution (1979–2018), has been widely adopted in various hydrological modelling applications (He, 2020; Sun et al., 2023).

In addition, several datasets were collected to describe the land surface characteristics (i.e., soil, topography, land cover type, and vegetation). Specifically, the soil texture (i.e., the proportions of sand, loam, and clay) and the bulk density of six soil  
 155 layers at depths between 0 and 200 cm were obtained from the SoilGrids1km dataset (Poggio et al., 2021). Topography was



characterized using the Shuttle Radar Topography Mission (SRTM) Digital Elevation Model (DEM) V4.1 (90 m resolution) (Jarvis et al., 2008) and land cover (14 classes) was derived from the University of Maryland's 1 km global dataset (UMD Land Cover; Hansen et al., 2021). Furthermore, monthly vegetation information—including the leaf area index (LAI), albedo, and partial vegetation cover fraction ( $f_{canopy}$ )—was calculated from multi-year data of several Moderate Resolution  
 160 Imaging Spectroradiometer (MODIS) products (MCD43D51.061, MOD13A3.061, and MOD15A2H.061). Following established methodologies,  $f_{canopy}$  can be derived from the Normalized Difference Vegetation Index (NDVI) using the formula provided by Bohn and Vivoni (2019):

$$f_{canopy} = \frac{NDVI - NDVI_{min}}{(NDVI_{max} - NDVI_{min})^2} \quad (1)$$

Then, the four-layer soil temperature from the ERA5 Land product is extracted and averaged to serve as the bottom  
 165 boundary condition for the soil heat flux in the VIC model (Muñoz Sabater et al., 2021). Collectively, the land surface characteristics are integrated into a standalone parameter file for VIC-5 model execution. This parameterization entails the conversion of land surface variables into model-specific parameters, as detailed in the following section.

Finally, for model calibration and evaluation, we retrieved the observed daily streamflow records from the five hydrological  
 170 stations (Fig. 1b), as published in the China Hydrological Yearbooks, and stored them in units of  $m^3s^{-1}$ . The datasets utilized in this study have varying temporal coverages; a common overlap period from 2003 to 2018 was therefore defined to ensure consistency in the modeling exercises, spanning the time during which all required model input data and streamflow records were available. Table 1 lists all the datasets used for deploying the VIC-5 model in this study.

**Table 1. An overview of the datasets used for deploying the VIC-5 model.**

Datasets	Description	Resolution	Reference
CMFD	Meteorological forcing dataset	$0.1^\circ \times 0.1^\circ$	He et al. (2020)
SoilGrids1km	Soil properties dataset	$1 \text{ km} \times 1 \text{ km}$	Hengl et al. (2014); Poggio et al. (2021)
SRTM DEM	Digital elevation dataset	$90 \text{ m} \times 90 \text{ m}$	Jarvis et al. (2008)
UMD Land Cover	Land cover dataset	$1 \text{ km} \times 1 \text{ km}$	Hansen et al. (2021)
MCD43D51.061 BSA	MODIS black sky albedo dataset	$1 \text{ km} \times 1 \text{ km}$	Schaaf and Wang (2021)
MOD13A3.061 NDVI	MODIS NDVI dataset	$1 \text{ km} \times 1 \text{ km}$	Didan (2021)
MOD15A2H.061 LAI	MODIS LAI dataset	$500 \text{ m} \times 500 \text{ m}$	Myneni et al. (2021)
ERA5 Land ST	ERA5 Land soil temperature dataset for four layers	$0.1^\circ \times 0.1^\circ$	Muñoz Sabater et al. (2021)



## 175 **3 Methodology**

### **3.1 Hydrological modelling**

The VIC model used for the hydrological simulation in this study was originally developed by Liang et al. (1994) as a land surface scheme within general circulation models (GCMs). As a physically based, spatially distributed hydrological model, it represents one of the most archetypal implementations of the FH69 blueprint (Freeze and Harlan, 1969), capable of  
180 simulating water and energy balances while accounting for the physical exchanges among the atmosphere, vegetation, and soil. The model is extensively used worldwide in studies of floods (Brunner et al., 2021), droughts (Lin et al., 2022), and broader water resource management (J S and Mishra, 2022). For brevity, a concise overview of the VIC model is presented here, highlighting the components most pertinent to the spatially distributed parameters considered in this study, with full details available elsewhere (Melsen et al., 2016; Hamman et al., 2018; Gou et al., 2020).

185

The VIC model employs a structured rectangular grid for spatial discretization, with each grid cell treated as an independent runoff generation unit without lateral interactions and assigned a distinct set of parameters to reflect land surface characteristics (i.e., land cover and soil). To represent sub-grid heterogeneity, the fractional coverage of each land cover type within a cell is modelled as a separate tile and the grid-scale response is derived by aggregating the contributions of all tiles  
190 using an area-weighted average. This stochastic, non-distributed modelling approach is sometimes referred to in the literature as the variability approach (Wen et al., 2012). Through the designed structure, the parameters in the VIC model possess a naturally capacity to represent spatial variability, allowing them to be physically linked to pre-compiled information such as topography, vegetation, and soil properties. As an illustration, the saturated hydrologic conductivity can be estimated from soil texture, following the empirical formulations proposed by Cosby Jr et al. (1984), as given below:

$$195 \quad \log K_s = 0.0126x - 0.0064y - 0.6 \quad (2)$$

where  $x$  denotes the sand content and  $y$  denotes the clay content. Overall, such transfer functions provide the conceptual foundation for regionalization approaches such as MPR.

The complete rainfall-runoff process comprises both runoff generation and routing stages. The RVIC model was proposed as  
200 a post-processor of the VIC model, designed to trace river channel flow by a pre-defined Unit Hydrograph (UH) and generate hydrographs at specified outlet points (Lohmann et al., 1996). The principle of RVIC can be briefly described as the solution of the linear Saint-Venant equations within a linear time-invariant system. Its primary parameters, flow velocity and diffusion coefficient, are generally treated either as spatially uniform free parameters to be calibrated or as fixed constants in the absence of observations. To date, RVIC remains the official extension of the VIC-5 and its earlier version, and has seen  
205 broad application (Shrestha et al., 2025).



Here, the VIC-5 image driver version and RVIC are consistently deployed at  $6 \text{ km} \times 6 \text{ km}$  spatial resolution (Fig. 1c) with a 3-hourly timestep, and the simulated output are aggregated to the daily timestep for calibration and evaluation. For the parameter estimation and calibration procedures, detailed descriptions are provided in the following sections.

### 210 3.2 Multiscale parameter regionalization with VIC-specific refinement

Samaniego et al. (2010) introduced a hierarchy of spatial scales to distinguish information across different resolution, which provides a basis for MPR implementation. Following this concept, we define the observational resolution describing land-surface characteristics as the level-0 scale (i.e., 1 km), while modelling resolution is represented by the level-1 scale (i.e., 6km), reflecting the principal process scale resolved by the model. As introduced before, the MPR technique is model-  
 215 independent, and its application to the VIC model requires specific refinement. Specifically, for each VIC parameter, we identify applicable prior transfer functions from literature and generalize them into a scale-independent form by incorporating the g-parameters. Using Eq. (2) as an example, we generalize it into the following form:

$$K_s = 10^{g_1 x + g_2 y + g_3} \quad (3)$$

where  $g_i$  constitutes a set of g-parameters to be calibrated. For clarity and tractability, refinement is applied exclusively to  
 220 several sensitive parameters (Gou et al., 2020), while the coefficients in the transfer functions of all other parameters are retained at their prior values (Mizukami et al., 2017), thus mitigating the issues arising from the curse of dimensionality. Table 2 summarizes the VIC-specific refinement of MPR. It is worth noting that VIC supports two equivalent baseflow parameterizations. Following Mizukami et al. (2017), we adopt the Nijssen formulation (i.e.,  $D_1$ ,  $D_2$  and  $D_3$ ) to avoid the parameter interactions present in the original Arno formulation. The derivation can be found in Nijssen et al. (2001).

225 **Table 2. VIC-specific refinement of MPR, detailing the transfer functions and the sources of the corresponding formulations.**

Parameter	Description	Predictors	Transfer function	Reference
$b$	The exponent of the variable infiltration capacity curve	Standard deviation of elevation ( $\sigma_{ele}$ )	$\frac{\log \sigma_{ele} - g_1}{\log \sigma_{ele} + 10 \cdot g_2}$	Dumenil and Todini (1992); Hurk and Viterbo (2003); Balsamo et al. (2009)
$D_1$	Linear reservoir coefficient [ $T^{-1}$ ]	Saturated hydrologic conductivity ( $K_s$ ); mean slope angle ( $S$ ); normalization factor of soil moisture ( $S_f$ ) set to one	$\frac{K_s \cdot S}{10^{g_3} \cdot S_f}$	Mizukami et al. (2017)
$D_2$	Nonlinear reservoir coefficient [ $L^{-2}T^{-1}$ ]	$K_s$ ; $S$ ; $S_f$	$\frac{K_s \cdot S}{10^{g_4} \cdot S_f^2}$	Mizukami et al. (2017)
$D_3$	Soil moisture depth at which baseflow transition occurs from linear to nonlinear [L]	Field capacity ( $\theta_c$ ); layer thickness of the third soil layer ( $h_3$ )	$g_5 \cdot \theta_{fc} \cdot h_3$	Mizukami et al. (2017)
$v$	Average flow velocity within each grid [ $LT^{-1}$ ]	Accumulated upstream area ( $acc$ ); $S$	$g_6 \cdot acc^{g_7} \cdot S^{g_8}$	K et al. (2005); Duc et al. (2007); Chen et al. (2019)
$D$	Average diffusion coefficient within each grid [ $L^2T^{-1}$ ]	Flow distance within each grid ( $d$ ); $velocity$	$g_9 \cdot d \cdot v$	Yang et al. (2016)

\*Note: Units are  $K_s$  ( $\text{mm s}^{-1}$ ),  $S$  (%),  $\theta_c$  ( $\text{m}^3 \text{ m}^{-3}$ ),  $h_3$  (m),  $acc$  ( $\text{km}^2$ ), and  $d$  (m).



Besides the spatially explicit parameterization of soil hydraulic-related parameters ( $b$ ,  $D_1$ ,  $D_2$ , and  $D_3$ ), two additional refinements were made to parameters that exert strong control on runoff generation and concentration. First, it is widely recognized among the VIC users that the vertically discretized soil depth is a key determinant of runoff generation. In the classic VIC-3L (i.e., VIC three-layer) configuration, the upper two soil layers respond rapidly to precipitation, generating surface flow according to the Xinanjiang formulation, whereas the bottom layer governs baseflow, resulting in a slower runoff response (Liang and Xie, 2001). Different soil layer thicknesses produce significantly different runoff responses; consequently, these thicknesses ( $d_1$ ,  $d_2$ , and  $d_3$ ) are typically treated as free parameters during calibration to fine-tune the VIC behavior (Gou et al., 2020). In order to feed soil data into the transfer function, it is necessary to reconcile the original soil-layer structure with the VIC vertical structure. As shown in Fig. 2, a two-step mechanism is applied here, involving aggregation and scaling. Aggregation allows the soil information to be represented in a standard three-layer form, determined by the layering numbers  $z_1$  and  $z_2$ . Scaling then multiplies the original thickness ( $d_o$ ) by  $g_{10}$ , providing VIC with the flexibility to adjust the final computational layer depths. This mechanism is applicable to most soil-column-based hydrological models and has been validated in Mizukami et al. (2017). However, previous implementations used domain-wide uniform values of  $z_1$ ,  $z_2$ , and  $g_{10}$ , a simplification that diminished the representation of spatial heterogeneity in soil layer depths and reflected the limited availability of spatially grounded information on vertical soil structure. In this study, we compare simulations using uniform depths with those employing subbasin-unique depths (i.e., subbasin-specific values of  $z_1$ ,  $z_2$ , and  $g_{10}$ ), analogous to a semi-distributed scheme, to examine how spatially explicit parameterization alter model behavior.

Second, the refinement is applied to the RVIC parameters, velocity ( $v$ ) and diffusion ( $D$ ), respectively. In previous studies, these two parameters were generally considered constant or spatially uniform free parameters to be calibrated (Shrestha et al., 2025; Yousefi Sohi et al., 2024). The official VIC documentation also recommends a diffusivity of 800 m<sup>2</sup>/s and a velocity of 1.5 m/s as acceptable values (<https://vic.readthedocs.io/en/vic.4.2.d/Documentation/Calibration>). Nonetheless, we use the MPR technique here to enhance the spatial representation of these two parameters by linking them to topography (Table. 2). This enhancement is then assessed for its impact on model behavior, which is particularly relevant for applications with limited prior information on channel routing, such as Manning's coefficients or channel morphology. Additionally, RVIC relies on UH as the impulse response function to convert runoff into streamflow, requiring them to be predefined. While various types of UH exist, such as the dimensionless SCS UH and the Nash UH (Roy and Thomas, 2016), the general UH (GUH) has drawn our attention due to its analytical formulation (Guo, 2022), with its expression presented as follows:

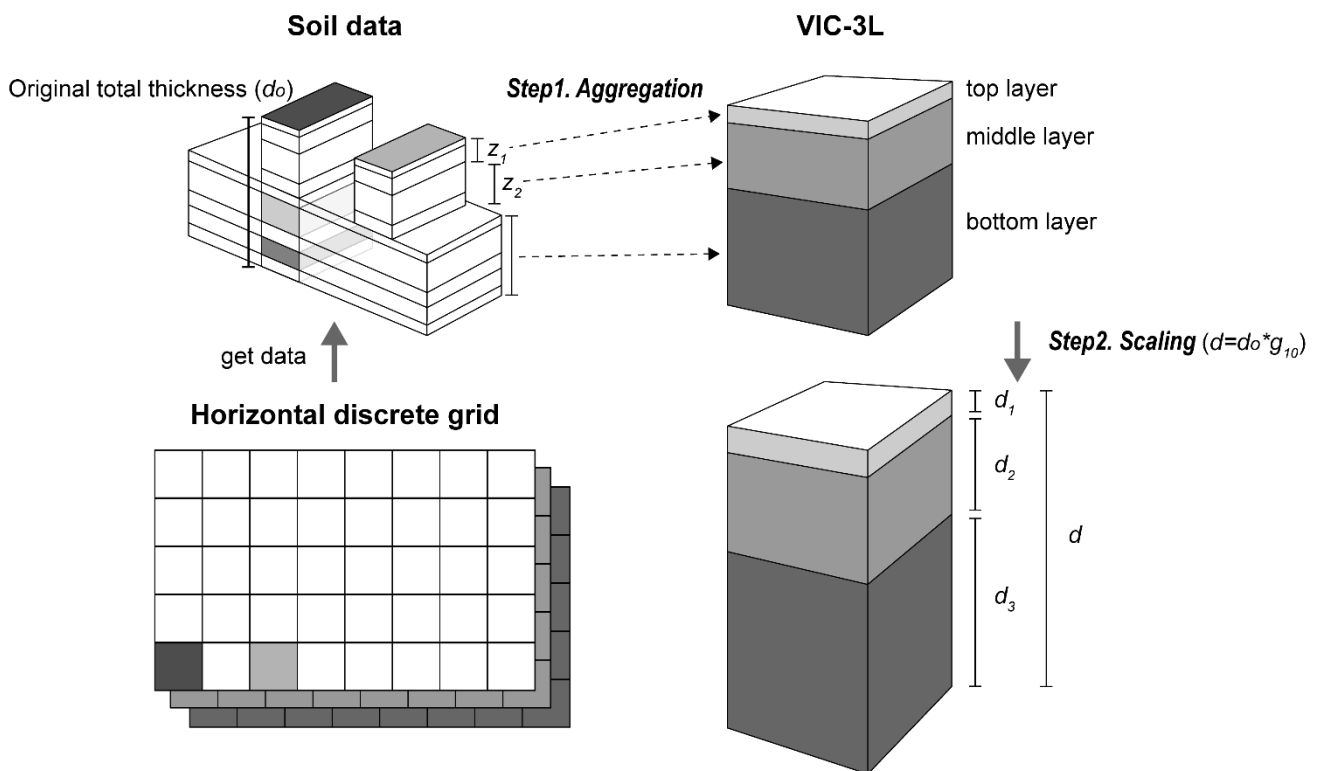
$$u(t) = \frac{dg}{dt} = \frac{\mu}{t_p} x(1 + mx)^{-(1+1/m)} \quad (4)$$

$$g(t) = 1 - (1 + mx)^{-1/m} \quad (5)$$

$$x(t) = \exp\left[\left(\mu\left(\frac{t}{t_p} - 1\right)\right)\right] \quad (6)$$



where  $t_p$  is the peak flow time;  $m$  is a dimensionless recessing coefficient that is determined by the downstream water surface condition; and  $\mu$  is the rising coefficient related to the basin characteristics. By calibrating the three parameters, the shape of the GUH can be freely adjusted, thereby providing flexibility in model representation when prior knowledge is limited. The GUH also demonstrate several advantages, including a solid theoretical and mathematical foundation (i.e., the solution of Chow’s linear hydrologic systems equations), the ability to reproduce typical flood responses with high accuracy, and, under certain conditions, the capacity to closely approximate traditional unit hydrographs. Based on this, we select it as the engine for RVIC, which acts as grid UH over the domain.



265

**Figure 2. Schematic of the two-step mechanism for reconciling soil data with VIC three-layer (VIC-3L) vertical structure. In the aggregation step, the original soil layers are merged into three VIC soil layers based on the layering numbers  $z_1$  and  $z_2$ . The scaling step then applies a scaling factor ( $g_{10}$ ) to the original total thickness ( $d_o$ ) to obtain the model-prepared layer thicknesses  $d_1$ ,  $d_2$ , and  $d_3$ .**

### 270 3.3 Experiment framework for spatially explicit parameterization and multi-gauge calibration

For this study, we design an Experiment Framework to evaluate the effect of Spatially explicit Parameterization and Multi-gauge calibration, termed EF-SPM (Fig. 3). The eight calibration cases, differing in their configurations of parameterization and calibration objectives, are summarized in Table 3. By grouping and comparing these cases, we can derive seven experiments with clearly defined objectives (Table 4), and can organize them into the following four main experimental



275 setups. For clarity and ease of understanding, the terms “distributed” and “spatially explicit” are used interchangeably below,  
unless otherwise noted.

### **Experiment 1. The added value of spatially explicit parameterization.**

280 This experiment compares the calibration process and simulations between the fully spatially explicit (distributed) and  
spatial uniform parameter configurations to identify the effects of spatially explicit parameterization on model behaviour.  
Here, the calibration objective was treated as the controlled condition. Cases 7 and 8 were compared under the single-gauge  
calibration, while Cases 1 and 5 were compared under the multi-gauge calibration.

### **Experiment 2. The role of multi-gauge calibration.**

285 With the parameterization scheme (Distributed vs. Uniform) as a controlled variable, this experiment assesses the advantage  
of multi-gauge calibration for parameter identification and model improvement, via comparisons between Case 5 and Case 8  
(distributed) and between Case 1 and Case 7 (uniform). Note that Exp. 1 and 2 are orthogonally designed to decouple the  
independent and interactive effects of spatial complexity and calibration strategy, which thus ensures a distinct and non-  
redundant comparison within a rigorous  $2 \times 2$  framework and thereby facilitates our exploration of the potential cross-  
290 benefits between these two methodological dimensions.

### **Experiment 3. Benefit of the additional MPR refinements.**

As outlined in the previous section, additional refinements were applied to the soil layer depths and RVIC parameters to  
enhance their spatial representativeness. This experiment evaluates the impact of this refinement strategy on model  
295 behaviour. Under controlled conditions, the contrast between Case 4 and Case 5 isolates the effect of spatially explicit soil  
layer depths (specifically, values assigned per the sub-basin delineation in Fig. 1c), while the progression from Case 3 to  
Case 2 to Case 4 quantifies the impact of progressively increased RVIC complexity.

### **Experiment 4. Performance Evolution from Baseline to Full-Complexity setup.**

300 Finally, the joint effects of these configurations are evaluated by comparing the simplest configuration (Case 6) against the  
most complex one (Case 5). As detailed in Table 5, the parameter count for the fully distributed parameterization is over  
double that of the fully uniform one. We anticipate that refining spatial representation of parameters will enhance model  
performance, yet also compromise parameter identifiability. Whether this can be paired with better calibration to enhance  
model realism is the key question we seek to answer.



305 **Table 3. Overview of the calibration cases with different configurations.**

No.	VIC parameters	Soil layer depths	RVIC parameters	Calibration objective
Case 1	Uniform	Uniform	Uniform	Multi-gauge
Case 2	Distributed	Uniform	Uniform	Multi-gauge
Case 3	Distributed	Uniform	Fixed constant	Multi-gauge
Case 4	Distributed	Uniform	Distributed	Multi-gauge
Case 5	Distributed	Distributed	Distributed	Multi-gauge
Case 6	Uniform	Uniform	Fixed constant	Single-gauge
Case 7	Uniform	Uniform	Uniform	Single-gauge
Case 8	Distributed	Distributed	Distributed	Single-gauge

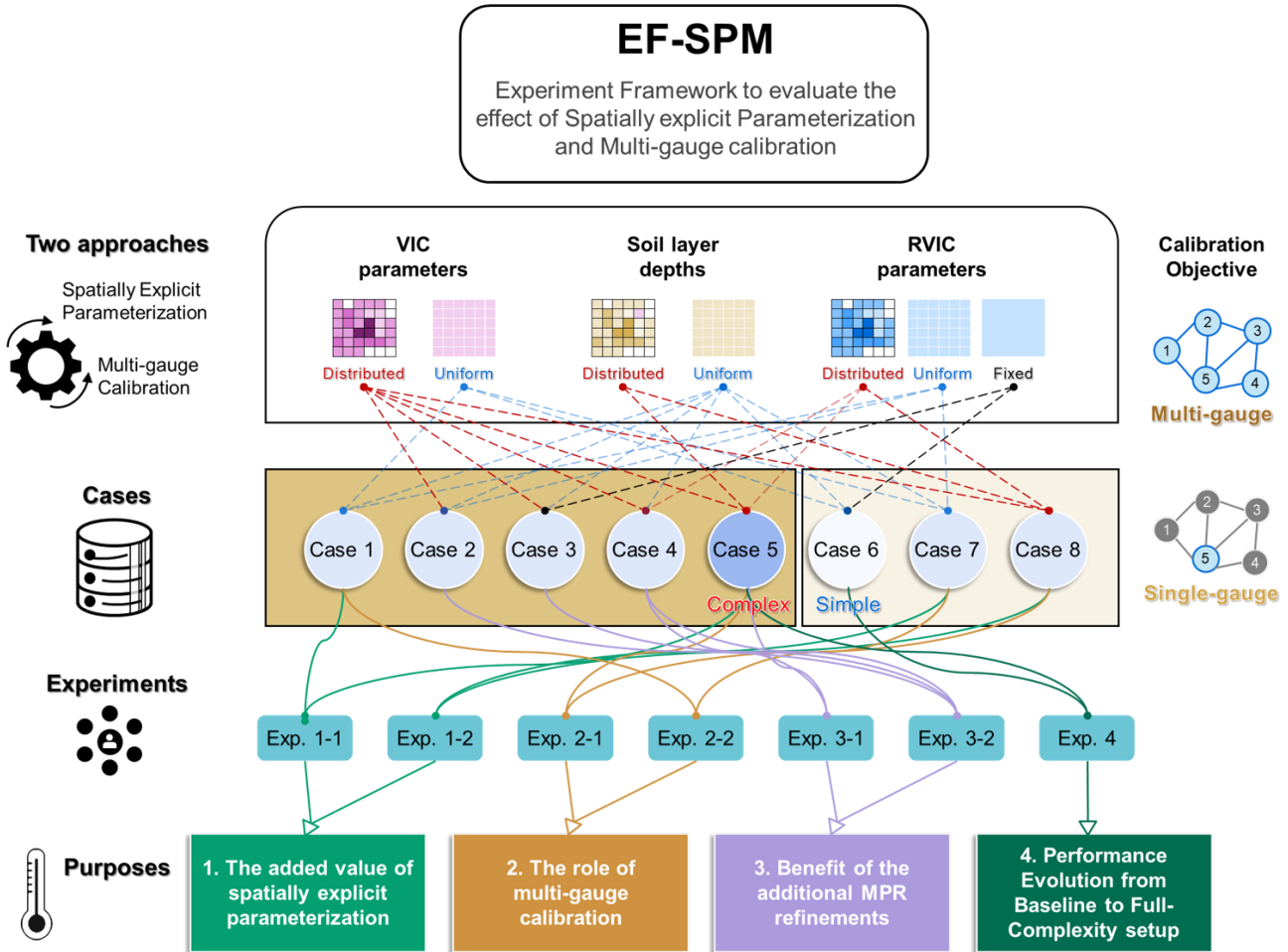
**Table 4. Summary of experiments within the EF-SPM framework, showing the cases considered, the configurations compared, and their purposes.**

Experiment	Cases	Defined purpose
Exp. 1-1	Case 1 and Case 5	Uniform vs. fully distributed parameterization (under multi-gauge calibration)
Exp. 1-2	Case 7 and Case 8	Uniform vs. fully distributed parameterization (under single-gauge calibration)
Exp. 2-1	Case 5 and Case 8	Multi-gauge vs. single-gauge calibration (under distributed parameterization)
Exp. 2-2	Case 1 and Case 7	Multi-gauge vs. single-gauge calibration (under uniform parameterization)
Exp. 3-1	Case 4 and Case 5	Uniform vs. spatially explicit soil layer depths parameterization
Exp. 3-2	Case 3, Case 2 and Case 4	Fixed vs. uniform vs. distributed RVIC parameterization
Exp. 4	Case 6 and Case 5	Simplest baseline vs. fully distributed parameterization, multi-gauge calibration

**Table 5. Parameter configurations and total counts for the uniform and distributed parameterization.**

Spatial type	VIC parameters	Soil layer depths	RVIC parameters	Total number of parameters
Uniform	$b, D_1, D_2, D_3$	$z_1, z_2, g_{10}$	$tp, m, \mu, v, D$	12
Distributed	$g_1-g_5$	$z_1, z_2, g_{10}$ (each sub-basin)	$tp, m, \mu, g_6-g_9$	27

\*Note: A total of five sub-basins are employed in this study.



310

**Figure 3. Schematic illustration of the Experiment Framework to evaluate the effect of Spatially explicit Parameterization and Multi-gauge calibration (EF-SPM).**

### 3.4 Optimization algorithms and evaluation metrics

Different algorithms were employed for single-objective and multi-objective calibration. For the former, we used the  
 315 Covariance Matrix Adaptation Evolution Strategy (CMA-ES; Hansen and Ostermeier, 2001), a global, single-objective  
 optimizer based on a generate-and-update paradigm that has demonstrated robust performance in hydrological model  
 calibration (Knoben et al., 2020; Aerts et al., 2024). For multi-objective calibration, we likewise adopted an evolution  
 strategy, the Non-dominated Sorting Genetic Algorithm II (NSGA-II), to ensure a fair comparison by minimizing  
 algorithmic bias. We implemented all optimization algorithms with the DEAP Python package (De Rainville et al., 2012;  
 320 Fortin et al., 2012). In addition, both optimizers were configured with an identical population size of 20 and shared the same  
 objective function: the modified Kling-Gupta efficiency (KGE) of the streamflow, with the only difference being the number  
 of gauges considered in each case, as given below (Aerts et al., 2022):



$$KGE = 1 - \sqrt{(r - 1)^2 + \left(\frac{\mu_{sim}}{\mu_{obs}} - 1\right)^2 + \left(\frac{\sigma_{sim}/\mu_{sim}}{\sigma_{obs}/\mu_{obs}} - 1\right)^2} \quad (7)$$

where  $r$  is the linear correlation coefficient between observed ( $obs$ ) and simulated flow ( $sim$ ), while  $\sigma$  and  $\mu$  denote their respective stand deviations and means. The three terms in Eq. (7) represent, respectively, the correlation between observations and simulations ( $r$ ), the bias in the mean ( $\beta$ ), and the bias in the variability ( $\gamma$ ). For both the KGE and its individual components, a value closer to 1 denotes better model performance, with 1 representing perfect agreement.

To further support a comprehensive evaluation, we additionally considered several signature metrics, as highlighted in the diagnostic evaluation framework (Gupta et al., 2008). Unlike aggregated performance metrics, hydrologic signatures offer a quantitative measure of specific hydrograph properties or behavior (e.g., total volume, flow peaks, and recession limbs). This allows for a more refined characterization of the temporal dynamics inherent in hydrography and helps pinpoint specific discrepancies in simulated flow patterns. Following Yilmaz et al. (2008) and Casper et al. (2012), a suite of flow duration curve (FDC)-based bias metrics was adopted. Specifically,  $\%PBias$  was used to characterize overall water volume differences;  $\%BiasFHV$  quantifies discrepancies in the high-flow segment;  $\%BiasFLV$  represents differences in the low-flow segment;  $\%BiasFMS$  describes deviations in the slope of the middle segment; and  $\%BiasFMM$  measures the percentage differences in mid-range flow levels. The corresponding formulations are given below:

$$\%PBias = \frac{\sum_{i=1}^N (Q_{sim}^i - Q_{obs}^i)}{\sum_{i=1}^N Q_{obs}^i} \times 100\% \quad (8)$$

$$\%BiasFHV = \frac{\sum_{h=1}^H (Q_{sim}^h - Q_{obs}^h)}{\sum_{h=1}^H Q_{obs}^h} \times 100\% \quad (9)$$

$$\%BiasFLV = \frac{\sum_{l=1}^L [\log(Q_{sim}^l) - \log(Q_{sim}^{min})] - \sum_{l=1}^L [\log(Q_{obs}^l) - \log(Q_{obs}^{min})]}{\sum_{l=1}^L [\log(Q_{obs}^l) - \log(Q_{obs}^{min})]} \times 100\% \quad (10)$$

$$\%BiasFMS = \frac{[\log(Q_{sim}^{m1}) - \log(Q_{sim}^{m2})] - [\log(Q_{obs}^{m1}) - \log(Q_{obs}^{m2})]}{[\log(Q_{obs}^{m1}) - \log(Q_{obs}^{m2})]} \times 100\% \quad (11)$$

$$\%BiasFMM = \frac{Median(Q_{sim}) - Median(Q_{obs})}{Median(Q_{obs})} \times 100\% \quad (12)$$

where  $Q$  denotes the streamflow;  $i = 1, 2, \dots, N$ ,  $h = 1, 2, \dots, H$ , and  $l = 1, 2, \dots, L$  are the indices of flow value in the full record, the high-flow segment (exceedance probabilities of 0-0.02 for  $\%BiasFHV_2$  and 0-0.01 for  $\%BiasFHV_1$ ), and low-flow segment (defined as 0.7-1.0) of the flow duration curve, respectively. The middle-flow segment is bounded by two thresholds,  $m1$  and  $m2$ , corresponding to exceedance probabilities of 0.2 and 0.7, respectively. Note that the original definitions were slightly modified here to ensure consistent sign conventions across all metrics, where negative values indicate an underestimation by the simulations.



350 The full period from 2003 to 2018 was allocated for warm-up (2003–2004), calibration (2005–2014), and validation (2015–  
2018) in a 1:5:2 ratio. To ensure computational efficiency while maintaining calibration performance, we conducted 40  
calibration trials for each case (amounting to 40 trials  $\times$  20 individuals = 800 model runs in total), a number we found  
sufficient to ensure convergence based on our preliminary tests. All cases implemented in this study were deployed using the  
Easy VIC Build (EVB) open-source Python framework developed by our team  
355 ([https://github.com/XudongZhengSteven/easy\\_vic\\_build](https://github.com/XudongZhengSteven/easy_vic_build)), which was designed to streamline the deployment process of the  
VIC model.

## 4 Results and discussion

### 4.1 Comparative overview of model performance

In this section, we first present an overview of the KGE-based streamflow simulation performance across all cases within the  
360 EF-SPM. To mitigate calibration uncertainty, the ensemble-mean KGE derived from the five optimal solution sets is  
reported, synthesizing results from multiple calibration trials (Table 6). As shown, Case 5 and 4 account for the first- and  
second-best performances in nearly all cases, for both calibration and validation. This behavior is in line with expectations,  
given that these cases involve a more explicit representation of spatial parameters and tighter calibration constraints. A  
comparable pattern of enhancement emerges when transitioning from simpler to more complex configurations (e.g., Case 6  
365 to Case 8, and Cases 1–3 to Cases 4–5). Notably, the most substantial performance gain was observed when moving from  
the simplest (Case 6) to the most complex configuration (Case 5), as anticipated in Exp. 4. In addition, a spatial dimension to  
performance differences was also observed, where upstream headwater sub-basins (e.g., Hanzhong and Youshui)  
consistently underperformed relative to downstream locations.

370 The initial analyses are encouraging, demonstrating that improvements in spatial parameter explicitness and multi-gauge  
calibration consistently lead to better streamflow reproduction. In particular, the overall simulation performance is  
satisfactory at the basin outlet (Shiquan station), with calibration KGE exceeding 0.76 across all cases and validation KGE  
values remaining above 0.67. The results presented here establish the context for analyzing the specific effects of these  
configuration.



375 **Table 6. Overview of ensemble mean performance metrics (KGE) for all calibration cases. Best values are highlighted in bold, with second-best values underlined.**

No.	Calibration period (2005–2014)					Validation period (2015–2018)				
	Hanzhong	Yangxian	Youshui	Lianghekou	Shiquan	Hanzhong	Yangxian	Youshui	Lianghekou	Shiquan
Case 1	0.410	0.630	0.487	0.653	0.763	0.504	0.604	0.370	0.614	0.686
Case 2	0.414	0.634	0.482	0.644	0.762	0.508	0.605	0.362	0.595	0.681
Case 3	<b>0.423</b>	0.638	0.492	0.653	0.760	0.518	0.605	0.379	0.608	0.678
Case 4	<u>0.418</u>	<b>0.657</b>	<b>0.533</b>	<u>0.715</u>	<b>0.787</b>	<u>0.521</u>	<u>0.637</u>	<b>0.446</b>	<u>0.730</u>	<u>0.689</u>
Case 5	0.415	<u>0.656</u>	<u>0.518</u>	<b>0.716</b>	<u>0.784</u>	<b>0.523</b>	<b>0.640</b>	<u>0.443</u>	<b>0.745</b>	<b>0.690</b>
Case 6	0.406	0.632	0.476	0.641	0.763	0.501	0.607	0.352	0.593	0.679
Case 7	0.405	0.630	0.476	0.641	0.763	0.500	0.606	0.353	0.595	0.683
Case 8	0.377	0.621	0.499	0.661	0.769	0.456	0.596	0.408	0.658	0.685

## 4.2 Spatially explicit parameterization: impact and trade-off analysis

The refinement of spatial representation involves three parameter groups: VIC parameters, soil layer depths, and RVIC parameters. To maintain analytical clarity, this section focuses solely on evaluating their combined effect on simulation in  
 380 Exp. 1 (Case 1 vs. Case 5 and Case 7 vs. Case 8), leaving the analysis of their individual effects from Exp. 3 to a subsequent section. Note that, for robustness, all results herein represent the ensemble values of the top five optimal solutions, consistent with the previous section.

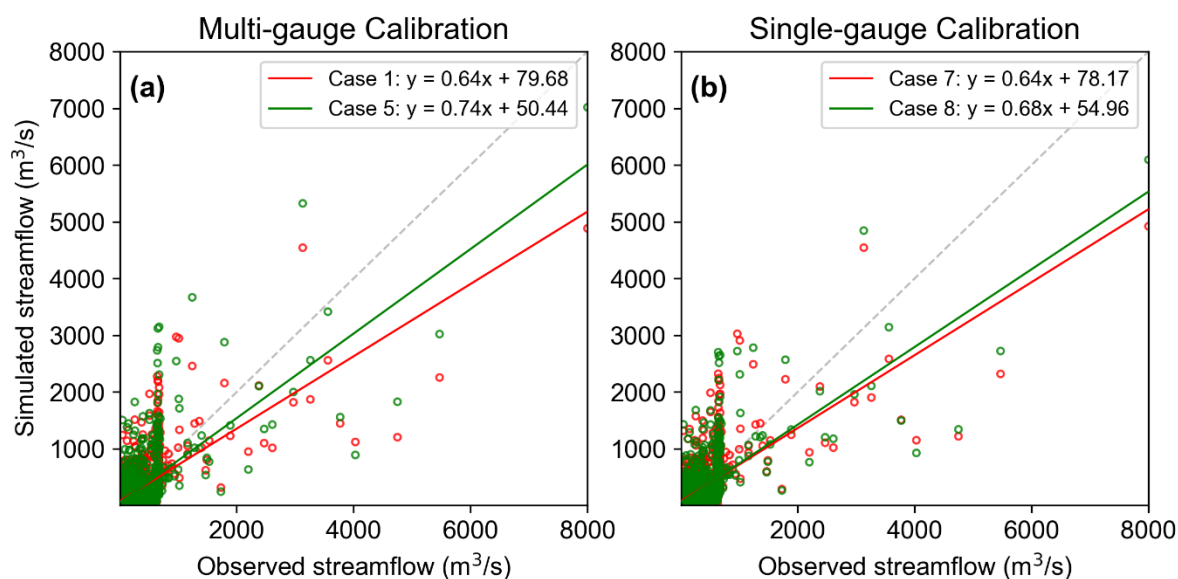
### 4.2.1 Hydrograph simulation

We first sought to determine whether enhanced spatial parameterization alters the behavior of the hydrograph – i.e., the  
 385 integrated hydrological response. A comparison of the overall simulation patterns for the four cases in Exp. 1 at the Shiquan station during the validation period, presented in the observed-simulated streamflow space in Fig. 4, indicates a consistent systematic underestimation bias across all configurations. Among these, the cases representing distributed parameterization (Cases 5 and 8, shown in green) visibly outperform those with uniform parameterization (shown in red), as demonstrated by their closer alignment with the 1:1 line. In terms of calibration strategy, the multi-gauge calibration appears to be superior.  
 390 This is exemplified by Case 5, which yields a regression slope of 0.74—the highest among all cases and closest to the ideal value of 1.

Next, we evaluated the simulation discrepancies across different hydrological conditions based on the FDCs (Ma et al., 2024), as presented in Fig. 5. A clear pattern is that, for the shared target station (Shiquan), FDCs align more closely under  
 395 the same parameterization (i.e., Case 1 with Case 7, and Case 5 with Case 8), suggesting that parameterization exerts a greater influence on the simulation pattern than calibration configuration. In general, spatially explicit parameterization

(Cases 5 and 8) offer improved simulation of the high-flow segment, yielding higher peak values; however, this comes at the expense of accurately capturing extreme low flows, namely, an overestimation of baseflow.

400 The signature metrics in Tables 7 and 8 provide quantitative support for the above behaviour at the Shiquan station: the shift from uniform to spatially explicit parameterization enhances  $\%BiasFHV_2$  by 5% and 7% (absolute change), and improves  $\%BiasFHV_1$  even more substantially (by 8% and 18%), while simultaneously worsening  $\%BiasFLV$  by 0.6% and 8.6%, under both multi-gauge and single-gauge calibration setups. Importantly, attention is drawn to the nearly universal improvement in the mid-FDC segment from Cases 1/7 to Cases 5/8. This consistent pattern across all stations provides  
 405 compelling evidence for the benefits afforded by spatially explicit parameterization. Additionally, single-gauge calibration shows a compensatory effect, where increasing model complexity improves high-flow simulation at the target gauge but degrades performance at all other sites (Table 8). This illustrates an under-constrained inverse problem, a limitation that is alleviated by multi-gauge calibration and will be explored in detail in a later section.



410 **Figure 4.** Scatterplots with least-squares regression lines comparing observed and simulated daily streamflow at the Shiquan station during the validation period, under different case configurations. The grey dashed line represents the 1:1 line.

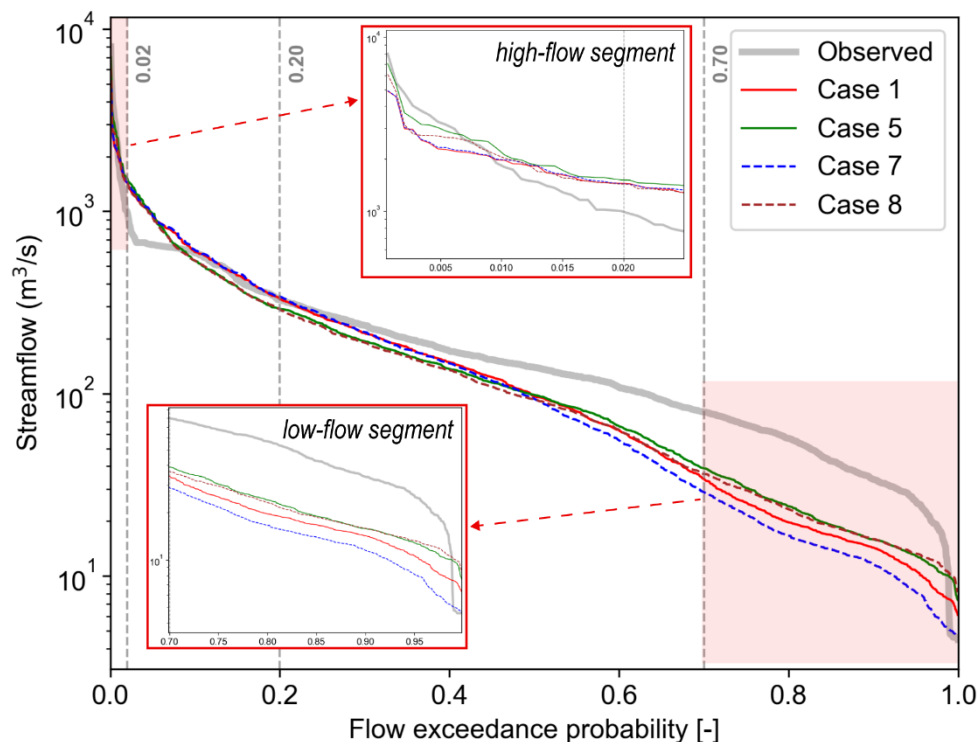


Figure 5. Comparison of observed and simulated flow duration curves for different case configurations at the Shiquan station during the validation period.

415 Table 7. Comparison of hydrologic signature metrics during the validation period under multi-gauge calibration: Case 1 versus Case 5. Bold values indicate where Case 5 shows improved performance relative to Case 1.

Metrics	Case 1 (Uniform)					Case 5 (Distributed)				
	Hanzhong	Yangxian	Youshui	Lianghekou	Shiquan	Hanzhong	Yangxian	Youshui	Lianghekou	Shiquan
%PBias	-44.2	-25.6	-43.7	-8.0	-3.6	<b>-41.4</b>	<b>-25.4</b>	-45.9	-9.3	-4.8
%BiasFHV <sub>2</sub>	-47.5	-40.5	-39.2	-1.9	-11.3	<b>-40.4</b>	<b>-33.8</b>	-47.4	-12.1	<b>4.2</b>
%BiasFHV <sub>1</sub>	-53.5	-47.5	-44.1	-6.9	-25.5	<b>-44.0</b>	<b>-38.3</b>	-52.6	-17.3	<b>-6.8</b>
%BiasFLV	0.7	16.2	-60.0	-19.7	-54.8	41.1	18.5	-67.1	<b>-14.3</b>	-55.4
%BiasFMS	85.2	79.3	20.3	81.9	60.6	<b>80.2</b>	<b>66.7</b>	<b>13.7</b>	<b>56.8</b>	<b>42.3</b>
%BiasFMM	-55.4	-36.8	-75.1	-38.1	-30.6	<b>-54.9</b>	<b>-35.8</b>	<b>-69.7</b>	<b>-24.1</b>	<b>-29.2</b>

\*Note: %BiasFHV<sub>2</sub> and %BiasFHV<sub>1</sub> are defined as the bias for the high-flow segment at exceedance probabilities of 0.02 and 0.01, respectively.



**Table 8. Comparison of hydrologic signature metrics during the validation period under single-gauge calibration: Case 7 versus Case 8. Bold values highlight where Case 8 outperforms Case 7.**

Metrics	Case 7 (Uniform)					Case 8 (Distributed)				
	Hanzhong	Yangxian	Youshui	Lianghekou	Shiquan	Hanzhong	Yangxian	Youshui	Lianghekou	Shiquan
%PBias	-44.2	-25.9	-43.6	-8.0	-3.7	-51.3	-29.4	-46.0	-13.0	-9.0
%BiasFHV <sub>2</sub>	-46.5	-39.9	-36.5	1.8	-10.2	-54.0	-43.3	-48.6	-17.6	<b>-5.1</b>
%BiasFHV <sub>1</sub>	-52.7	-46.8	-41.9	-3.3	-24.8	-59.0	-48.0	-54.0	-26.1	<b>-16.8</b>
%BiasFLV	18.0	37.2	-55.9	-9.6	-51.8	-37.9	<b>-11.3</b>	-69.6	-13.3	-60.4
%BiasFMS	106.4	92.5	31.0	95.1	74.6	<b>57.7</b>	<b>64.0</b>	<b>17.9</b>	<b>61.9</b>	<b>46.7</b>
%BiasFMM	-59.6	-42.1	-78.9	-47.9	-32.5	<b>-55.9</b>	<b>-39.2</b>	<b>-72.4</b>	<b>-29.9</b>	-33.3

#### 420 4.2.2 Water balance simulation

We now examine the differences in simulated water balance components at the watershed scale under the enhanced model with spatially explicit parameterization. Here, four major components (i.e., surface runoff, baseflow, evaporation, and soil water storage change) in the VIC model are spatially averaged over the entire watershed and aggregated over the validation period, with soil water storage change summed in absolute terms. This allows us to derive the relative contributions of each component, which are summarized as a pie chart in Fig. 6. A key finding in this synthesis is a marked shift in runoff partitioning from Cases 1/7 to Cases 5/8, characterized by a substantial decrease in baseflow and a concurrent, commensurate increase in surface runoff. This redistribution is consistent with, and provides a process-based explanation for, the previously noted improvement in high-flow simulation. It reveals the definitive influence of the spatially explicit parameterization scheme, which affects runoff generation processes by integrating spatial soil and terrain data into parameter estimation and provides greater flexibility in discretizing the vertical soil profile.

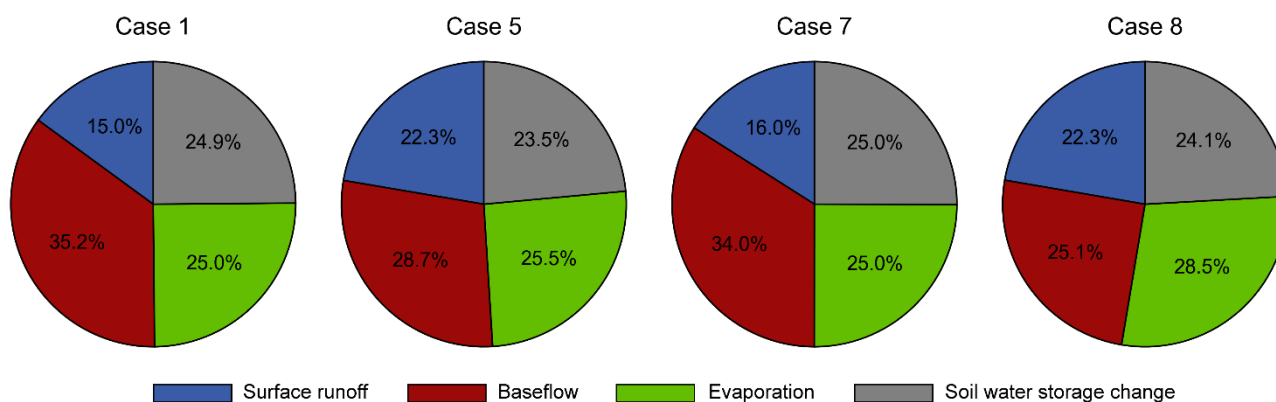


**Figure 6. Relative contributions of four major water balance components for different case configurations during the validation period.**



### 4.2.3 Spatial pattern simulation

435 Having identified shifts in bulk runoff partitioning, we, as a matter of course, proceed to examine their spatial manifestations. The central curiosity is the extent to which spatially explicit parameterization regulates the representation of spatial heterogeneity in hydrological processes compared to a uniform method. This leads us to examine the differences in surface runoff and baseflow between the two configurations, as shown in Fig. 7. Clearly, the improved spatial parameterization systematically increases surface runoff and decreases baseflow across the entire modelling domain, a result consistent with

440 prior findings. More significantly, this shift exhibits a blended spatial pattern, driven by sub-basin delineation according to soil layer depths (which enhances modulation in mid- to upper-stream sub-basins), and modulated by grid-scale variations in soil and topography (which attenuate differences in the low-elevation valleys of the midstream region). We argue that this spatially refined modulation of runoff generation is beneficial, at least for simulating medium to high flows, supported by the preceding analysis.

445

To conclude, the spatially explicit parameterization exerts a pronounced influence on hydrological simulations, as reflected in outlet hydrographs, runoff partitioning, and spatial distributions. This enhancement significantly benefits medium-to-high flow simulations but compromises extreme low-flow accuracy. Under single-gauge calibration, the potential risk of parameter under-constraint increases, which can in turn lead to degradation in runoff simulations for non-target sub-basins,

450 highlighting the nuanced trade-offs between model complexity and overall fidelity. The following section assesses whether spatially explicit parameterization exacerbates equifinality.

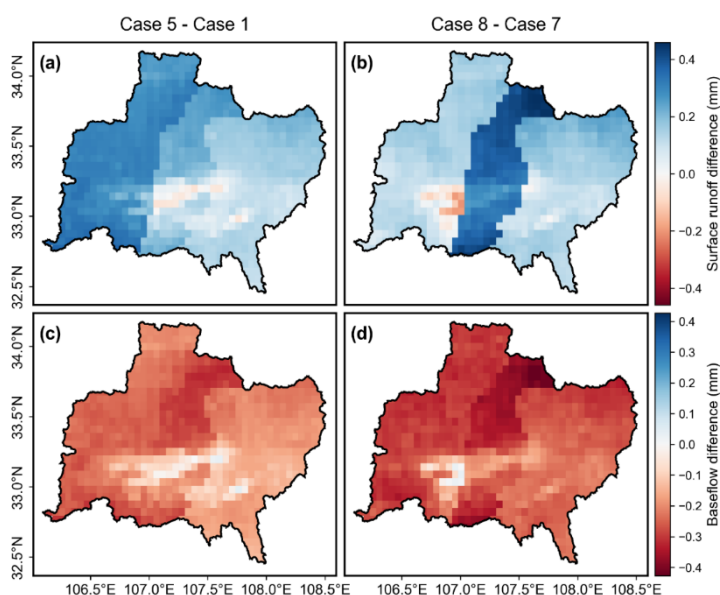


**Figure 7. Spatial distribution of differences in (a, b) surface runoff and (c, d) baseflow volumes between the two parameterization schemes over the validation period. Differences are calculated as spatially explicit minus uniform parameterization.**



#### 455 **4.3 Revealed perspectives from multi-gauge calibration**

This section delves into the parameter identifiability and calibration process to determine, via a comparative analysis (Exp. 2-1: Case 5 vs. Case 8, Exp. 2-2: Case 1 vs. Case 7), whether multi-gauge calibration confers a distinct advantage over its single-site counterpart and to investigate any cross-effect with the spatially explicit parameterization.

##### **4.3.1 Identifiability of parameters**

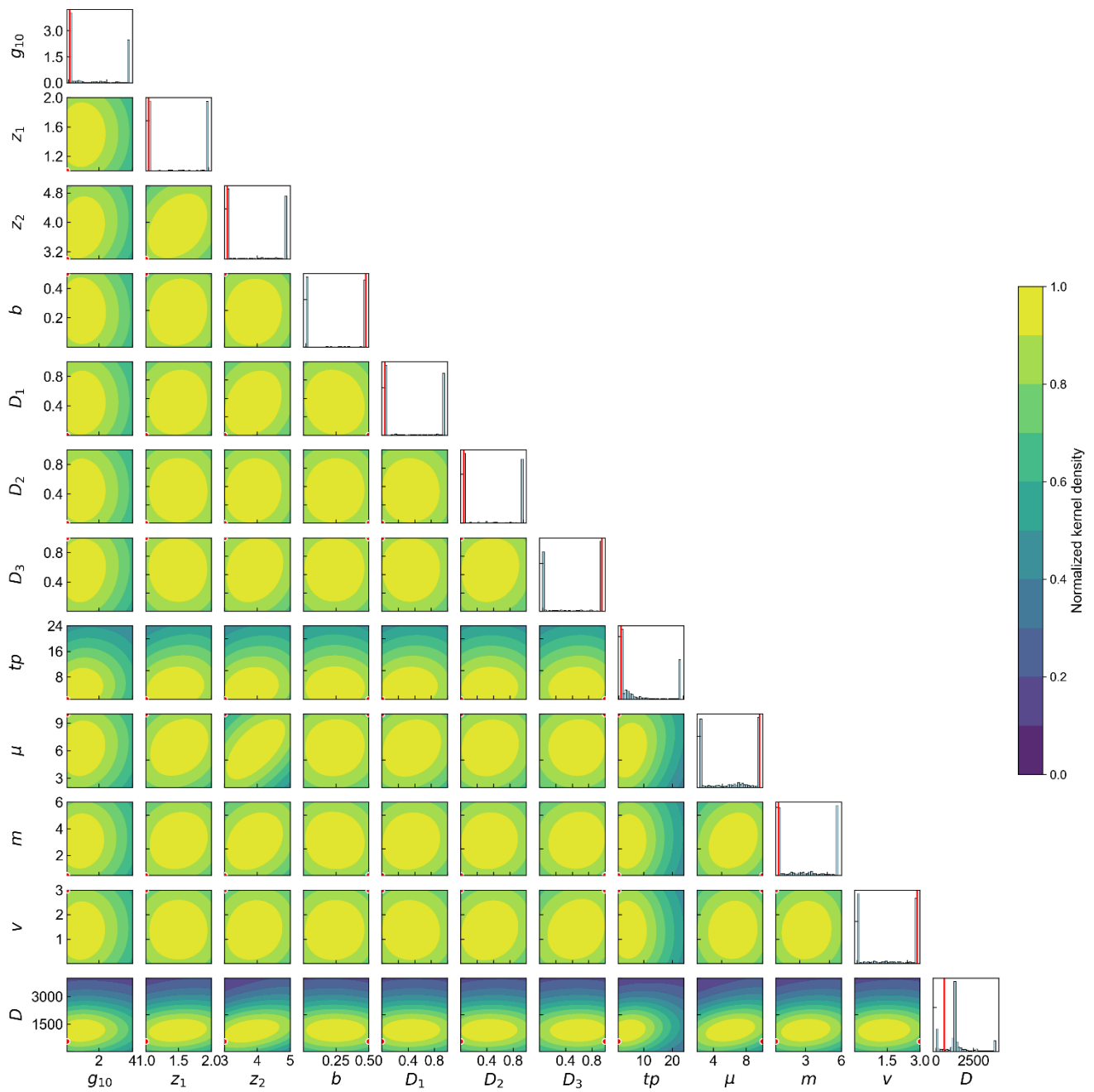
460 The inverse problem of hydrological model calibration is often ill-posed due to insufficient constraints. The under-constrained condition gives rise to equifinality, where distinct parameter sets yield nearly identical model responses, thereby complicating the identification of an optimal parameter set. A particularly concerning consequence of this equifinality is the problem of “right answers for all of the wrong reasons.” This issue has prompted extensive discussion on parameter identifiability within the hydrological community (Kittel et al., 2018; Aerts et al., 2024; Talbot et al., 2025).

465

Parameter identifiability, simply put, refers to the ease of isolating an optimal parameter set within the parameter space. By examining the relative positions of the optimal parameters and the sampled candidate solutions across the entire calibration process within the parameter space, we can investigate how identifiability is shaped by model complexity (i.e., spatial configuration of parameters) and by the formulation of the inverse problem (i.e., the calibration setup). Our comparative analysis reveals that, in contrast to Case 7 (Fig. 8), Case 1 exhibits a more concentrated kernel density distribution, with its optimal parameters consistently located near the region of highest frequency (Fig. 9). A similar finding is also observed when comparing Case 8 to Case 5, as detailed in Figs. S1 and S2 of the Supplementary Material. Therefore, we can reasonably conclude that multi-gauge calibration yields better-constrained solutions, leading to a significant enhancement in model parameter identifiability. From a theoretical perspective, this pattern arises from the use of globally shared free parameters (e.g., the  $b$  parameter under uniform settings and the  $g$  parameter in the MPR scheme), whose spatial compensation effects are mitigated through multi-gauge calibration (Liu et al., 2012). Furthermore, a comparison of Fig. 8 and Fig. S1 indicates a weakening in the clustering of background contours for Case 5. This weakening suggests that the spatially explicit parameterization, while enhancing spatial representational capacity, also expands the parameter set, reduces parameter identifiability, and consequently exacerbate model equifinality.

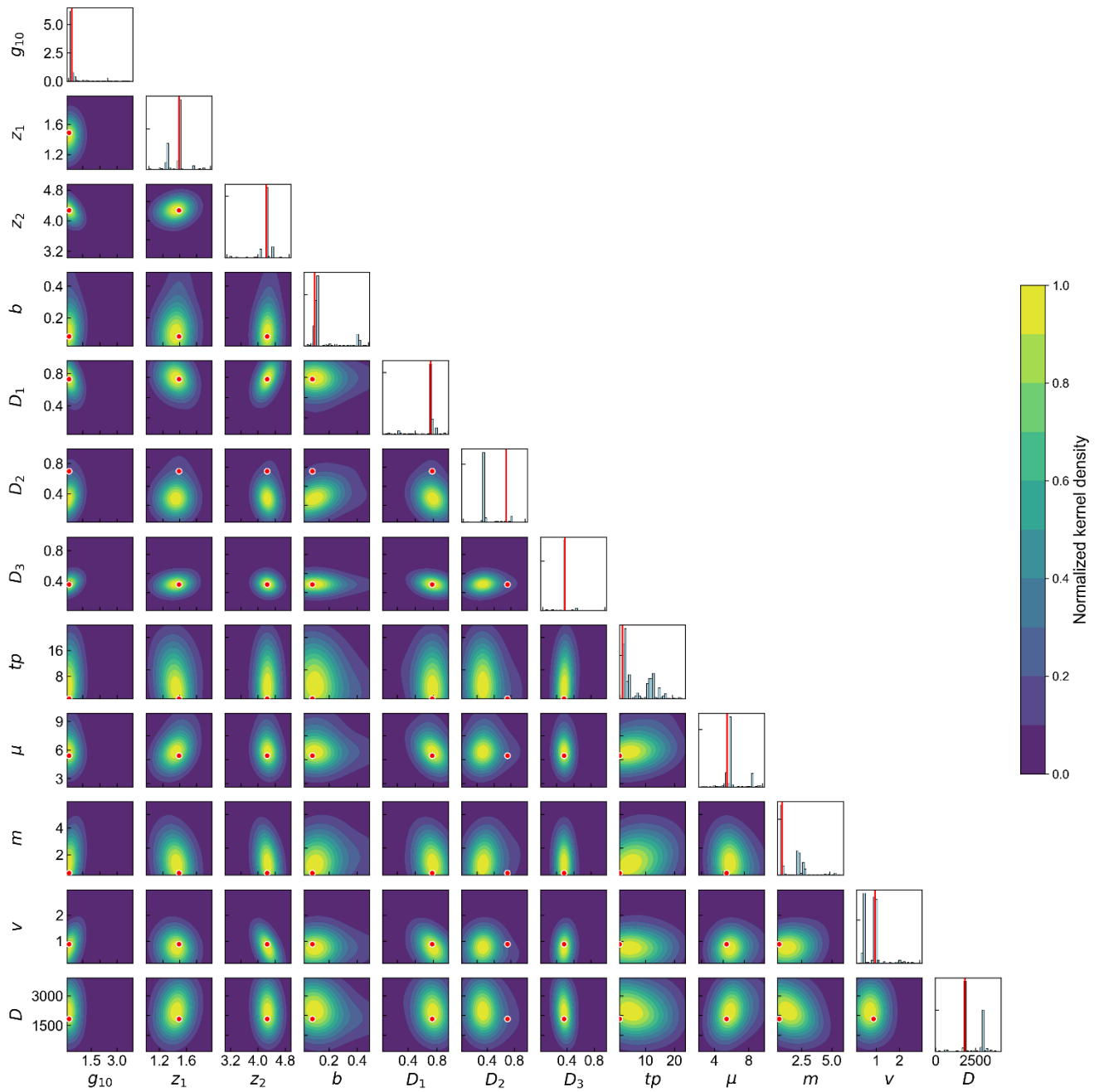
470

475



480

**Figure 8.** Post-calibration parameter distributions for Case 7. The optimal parameters are shown as red dots and lines. The background contours represent the standardized kernel density estimate derived from all candidate solutions, where yellow shading corresponds to high probability density regions. The histograms along the diagonal represent the marginal distribution of each individual parameter.



485

**Figure 9. Post-calibration parameter distributions for Case 1, following the same visualization conventions as Fig. 8. While the overall structure is similar, Case 1 exhibits more concentrated posterior distributions and different optimal values.**



#### 4.3.2 Cross-benefits of multi-gauge calibration and spatially explicit parameterization

490 Following the demonstrated advantages of multi-gauge calibration, we now turn to a pivotal follow-up question: what cross-  
benefits does spatially explicit parameterization confer, aside from its potential drawback of reduced identifiability?  
Addressing this is crucial for explaining the performance advantage of Case 5 over Case 1 (Table 6), despite the fact that  
they share the same calibration configuration and that Case 5 appears to pose greater calibration challenges (Fig. S2). Note  
that, from an experimental design perspective, we have grouped this section into Exp. 1-1 for the sake of simplified  
categorization.

495

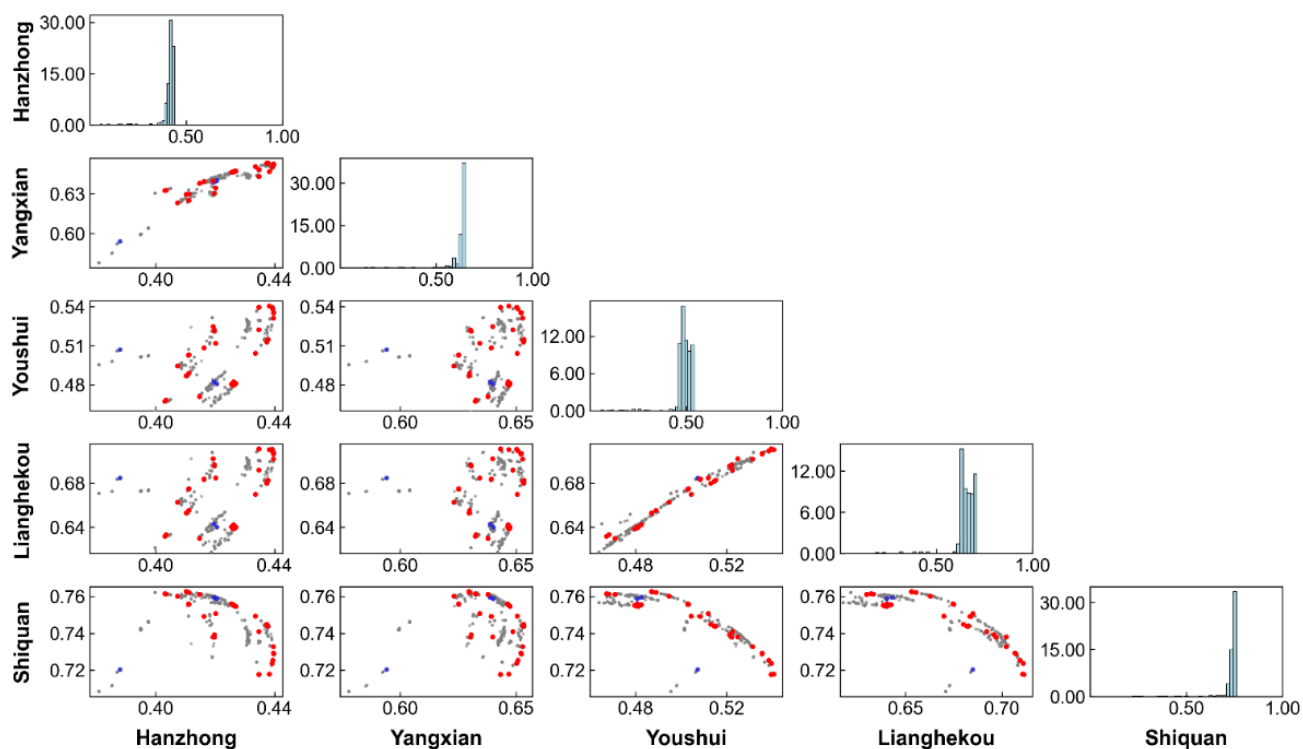
To answer the above question, we visualize the objective space for Cases 1 and 5 using multi-objective scatter plot matrices,  
as shown in Figs. 10 and 11. Interestingly, under the uniform parameter configuration (Case 1), the objectives exhibit  
pronounced trade-offs, manifested by continuous and convex arc-shaped Pareto fronts formed by the point clouds. In  
particular, gains in streamflow performance at Shiquan station degraded simulations at other sites (last row of Fig. 10). This  
500 phenomenon is consistent with our earlier finding of a compensatory effect under single-gauge calibration (Table 8), an  
outcome that is clearly detrimental to model realism. In contrast, when shifting to the spatially explicit parameterization in  
Case 5, the trade-off relationships were remarkably alleviated, accompanied by a broader dispersion of solutions in the  
objective space (Fig. 11), which can be interpreted as indicative of a more exhaustive calibration search that helps avoid  
entrapment in local optima.

505

Taken together, cross-benefit from spatially explicit parameterization combined with multi-gauge calibration are witnessed.  
This synergy indicates that enhancing spatial representation and imposing stronger constraints are mutually reinforcing.  
Improvements in either aspect alone exhibit clear limitations. For example, enhancing spatial representation without  
sufficient constraints can severely degrade parameter identifiability (as in Case 8). This provides a rationale for why, as  
510 hydrological models evolve from lumped to increasingly complex distributed formulations, parameter equifinality has gained  
growing attention (Wambura et al., 2018). Against this backdrop, multi-objective calibration is gradually emerging as a  
standard paradigm within the contemporary hydrological community. Conversely, relying solely on increased constraints  
while lacking adequate representation may intensify undesirable trade-offs among objectives (as in Case 1). This  
phenomenon is also reflected in prior literature, where studies have found that incorporating variables such as evaporation,  
515 soil moisture, or total water storage alongside streamflow in model calibration can degrade streamflow simulation  
performance—a typical trade-off that highlights potential structural limitations of model (Széles et al., 2020; Mei et al., 2023;  
Talbot et al., 2025). While existing work has largely been diagnostic in identifying this limitation, our study adopts a  
comparative framework (EF-SPM) to more explicitly reveal the conditions and mechanisms underlying the trade-off and  
cross-benefit. Building on this, we contend that the next phase of model development will undoubtedly involve deeper



520 integration with data and an increased emphasis on realism. This requires parallel advancements in both model  
representation and observational constraints, culminating in a robust framework for Model-Data Infusion.



525

**Figure 10.** Objective space scatter plot matrix for Case 1. The matrix depicts the trade-offs between calibration objectives, where each axis corresponds to the Kling-Gupta Efficiency (KGE) of simulated streamflow for a sub-basin (gauge). Grey dots represent all candidate solutions from the calibration process. The initial and final Pareto fronts are highlighted in blue and red, respectively. Histograms along the diagonal show the distribution of the KGE for each individual objective.

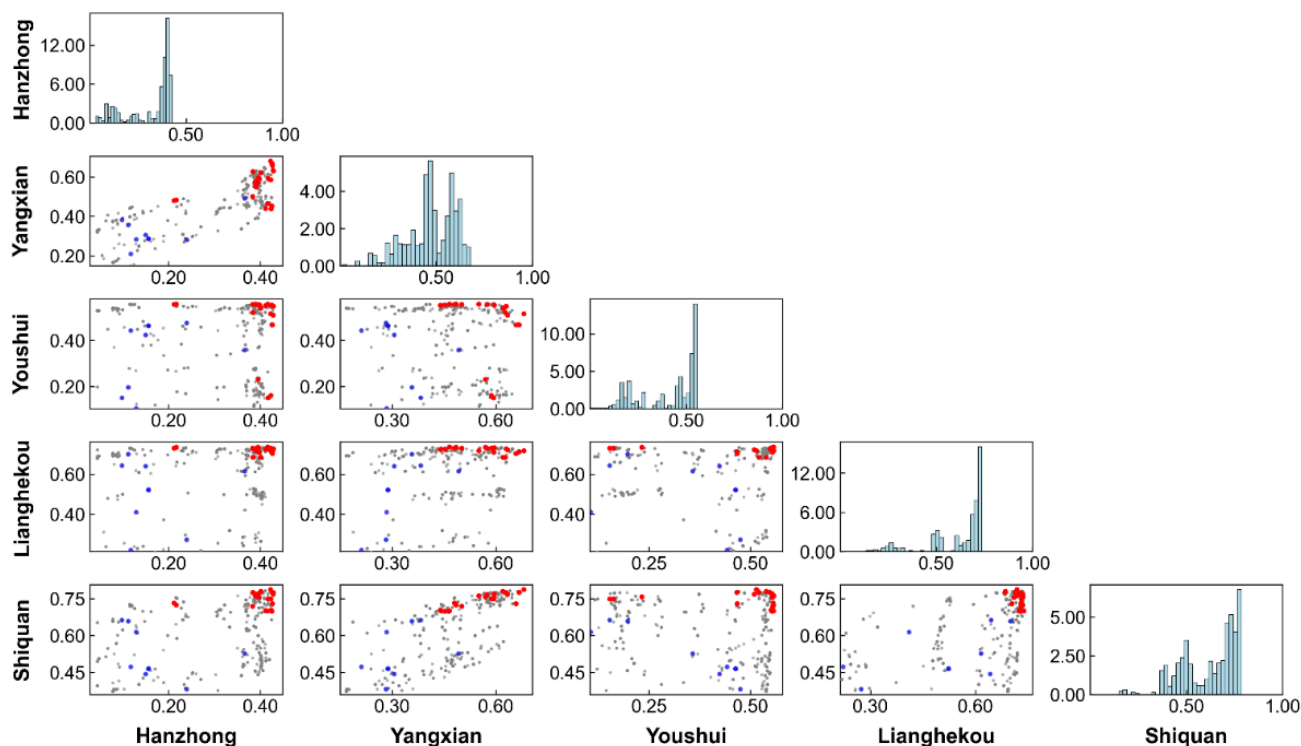


Figure 11. Objective space scatter plot matrix for Case 5, following the same visualization conventions as Fig. 10. In contrast to uniform parameter case, the trade-off relationships among objectives are substantially improved, and the solutions are more widely dispersed across the objective space.

530

#### 4.4 Individual effects from additional MPR refinements.

For completeness, this section investigates the individual effects of additional MPR refinements (the focus of Exp. 3) on hydrological simulations through specific case comparisons, considering two aspects respectively: soil layer depths (Exp. 3-1: Case 4 vs. Case 5) and the RVIC parameter (Exp. 3-2: Case 2 vs. Case 3 vs. Case 4). To ensure consistency between parameters and simulations, the top-ranked solution is adopted for analysis here rather than the ensemble values.

535

##### 4.4.1 Spatial discretization of soil layer depths at sub-basin level

The spatial characterization of soil depth in the MPR-VIC modelling framework was refined via a sub-basin discretization scheme, with independent parameter sets (i.e.,  $z_1$ ,  $z_2$ ,  $g_{10}$ ) allocated to each sub-basin. From Table 6, Case 4 shows a slight advantage in the calibration period and Case 5 in the validation period, although the distinction is minimal. It is argued that the aggregated metrics encapsulate not only the effect of soil layer depths but also the influence of the jointly calibrated RVIC parameters (i.e., routing process). To disentangle these effects, analysis is focused on the contrasting runoff generation process between the two cases.

540



According to Fig. 12, Case 5 produces lower spatially averaged soil moisture throughout the year in the upper and middle  
545 layers compared to the Case 4, with only minor differences in runoff-related components at the basin scale. However, the  
heterogeneity in runoff generation resulting from the parameterization of soil layer depths is clearly evident in space. As can  
be observed in Fig. 13 (which shows the differences for Case 5 vs. Case 4), the middle-upper sub-basins (Hanzhong,  
Yangxian) experience a significant increase in surface runoff alongside a decrease in baseflow, whereas the downstream sub-  
basins (Youshui, Lianghekou, Shiquan) display the reverse change. This can be intuitively explained by the discrepancies in  
550 vertical discretization. In the two upper sub-basins, Case 5 maintains the same vertical layering depths ( $z_1, z_2$ ) as Case 4 but  
applies a significantly reduced scaling factor ( $g_{10}$ ), resulting in thinner soil layers (Table 9). This reduction promotes greater  
surface runoff and diminished baseflow, a direct impact of soil thickness on hydrological simulation that has been  
demonstrated in several previous studies (Gou et al., 2020; Yeste et al., 2024). As a result, the simulated mean streamflow at  
the two upstream stations showed distinct improvement, with the  $\beta$  component of the KGE increasing from 0.447 and 0.704  
555 to 0.463 and 0.705, respectively. For the Youshui sub-basin, the substantially increase in scaling factor reduced both surface  
runoff and baseflow, owing to the enhanced storage capacity of the deepened third layer. The behaviour of the downstream  
stations differs most significantly between Case 5 and Case 4. Although the total soil thickness is reduced in Case 5, the  
change in  $z_2$  reallocates the depth distribution, yielding a relatively thicker middle layer ( $d_2$ ) and a thinner third layer ( $d_3$ ).  
Consequently, surface runoff decreases whereas baseflow increases, which contributes to an improved overall correlation ( $\gamma$ )  
560 in the streamflow time series (Table 9).

Several limitations of the current analysis should be noted. First, the differences in vertical soil layering affect not only the  
layer thicknesses but also the aggregated soil properties (Fig. 2). This, in turn, leads to variations in parameters such as  $D_1$ ,  
 $D_2$ , and  $D_3$ , as these parameters depend on the layer-specific soil hydraulic properties (e.g.,  $K_s$ ). Nevertheless, these  
565 secondary effects are not analysed further through controlled variable comparisons, owing to their intricately coupled nature.  
Second, the calibrated results for Case 5 are not considered the definitive optimum, as the calibration was limited to only 40  
trials due to available computational resources. Further optimization may yield more distinct vertical layering configurations,  
which we reserve for future investigation. Finally, we avoid basing the superiority of Case 4 or Case 5 exclusively on outlet  
flow performance. Such a single metric is inadequate because it masks not only the equifinality inherent in the joint  
570 calibration of VIC parameters, but also the complex interdependencies within the river network—where improvements in  
upstream simulations may compromise downstream accuracy. Nevertheless, the analysis above provides a clear indication  
that Case 5 exhibits improved spatial representativeness and flexibility compared to Case 4 at the sub-basin scale. In the  
absence of strong prior knowledge, discretization of soil layer depths at the grid-cell scale is nearly infeasible. A more  
pragmatic path forward, however, would be to cluster grid cells based on salient landscape attributes (e.g., elevation), an  
575 approach which we intend to explore in future work.

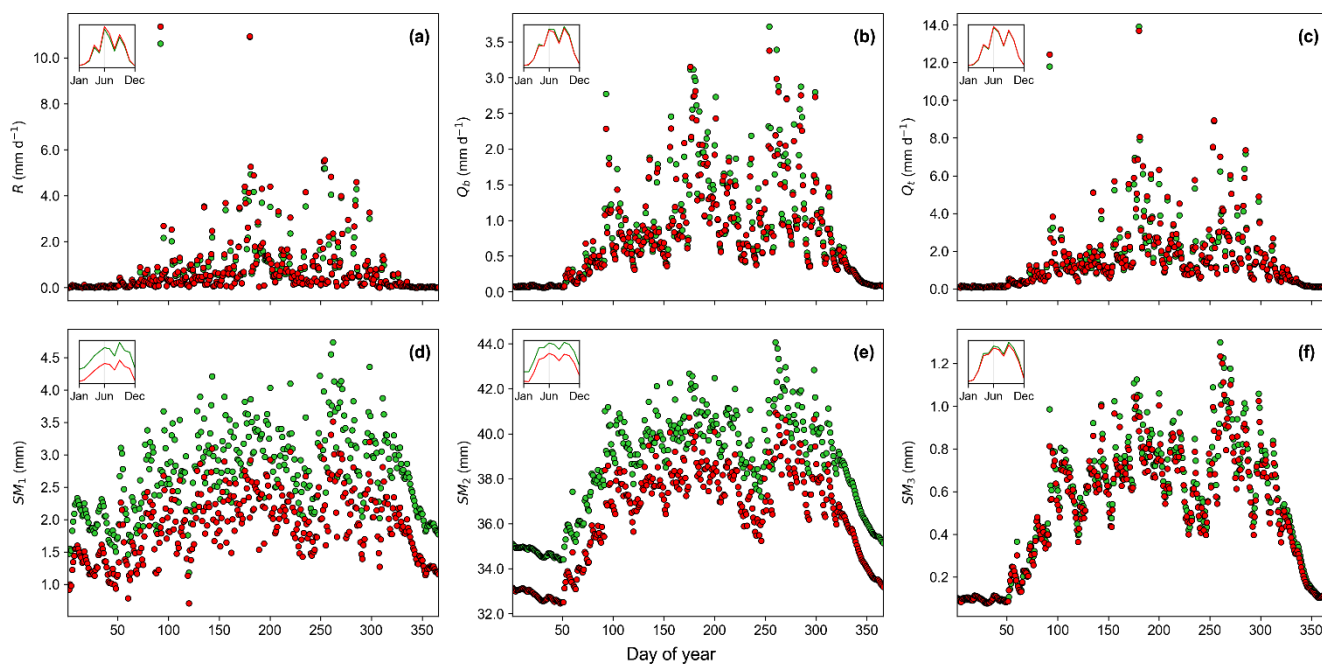
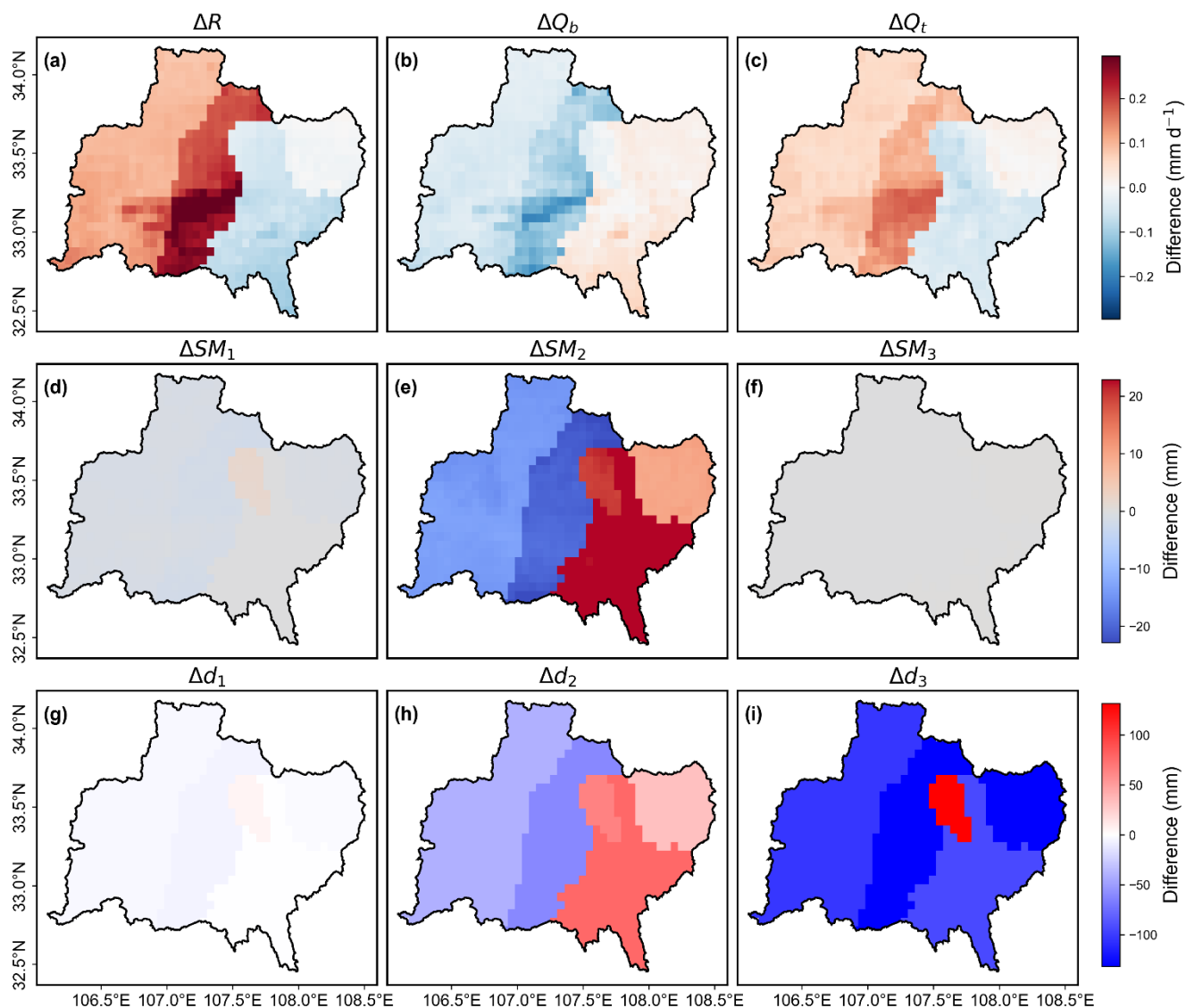


Figure 12. Long-term daily climatology of simulated hydrological variables for Case 4 (green) and Case 5 (red). The primary variables are: (a) surface runoff ( $R$ ), (b) baseflow ( $Q_b$ ), (c) total runoff ( $Q_t$ ), and (d–f) soil moisture in the top, middle, and bottom layers ( $SM_1$ ,  $SM_2$ ,  $SM_3$ ), respectively. Insets in the upper-left corners show the corresponding mean monthly climatology for each variable.

580



**Figure 13.** Spatial distribution of differences in long-term mean simulated variables during the validation period and soil layer depths between Case 4 and Case 5. Differences are shown for (a–c) surface runoff, baseflow, and total runoff, and (d–f) soil moisture in layers 1–3, respectively (variable definitions as in Fig. 12). The bottom row presents the corresponding differences in the calibrated soil layer depths: (g–i) Depths differences for soil layers 1–3 ( $\Delta d_1$ ,  $\Delta d_2$ ,  $\Delta d_3$ ). Positive values indicate higher magnitudes in Case 5 relative to Case 4.

585



**Table 9. Comparison of soil vertical layering parameters and signature metrics during the validation period: Case 4 versus Case 5. Bold values indicate an increase in the parameter value or a performance improvement for Case 5 relative to Case 4.**

	Case 4					Case 5				
	Hanzhong	Yangxian	Youshui	Lianghekou	Shiquan	Hanzhong	Yangxian	Youshui	Lianghekou	Shiquan
$g_{10}$	0.212	0.212	0.212	0.212	0.212	0.139	0.101	<b>0.330</b>	0.147	0.204
$z_1$	1.000	1.000	1.000	1.000	1.000	1.000	1.000	1.000	1.000	1.000
$z_2$	4.000	4.000	4.000	4.000	4.000	4.000	4.000	4.000	<b>5.000</b>	<b>5.000</b>
$r$	0.835	0.833	0.737	0.829	0.814	0.818	0.83	<b>0.739</b>	<b>0.844</b>	<b>0.821</b>
$\beta$	0.447	0.704	0.637	0.813	0.897	<b>0.463</b>	<b>0.705</b>	0.616	0.804	0.887
$\gamma$	1.076	0.954	0.868	0.869	1.011	1.142	<b>0.991</b>	<b>0.872</b>	0.865	1.039

#### 4.4.2 Spatialization scheme for RVIC parameters at the grid level

590 Cases 3, 2, and 4—defined by constant, uniform, and distributed parameters, respectively—form a gradient of increasing complexity in RVIC model parameterization. We assess the potential benefits corresponding to this parametric refinement. To factor out the effect of runoff generation, all three cases were run with an identical set of runoff generation parameters from the simplest Case 3 configuration, altering only the runoff concentration parameters. Their performance was then evaluated. Interestingly, this approach yielded results that diverged from the established benchmarks (Table 6). As shown in

595 Table 10, a consistent performance ranking was observed across all sub-basins, with Case 4 demonstrating superior performance, followed by Case 3 and then Case 2. This finding provides two key insights into the model behaviour. First, it highlights the effect of joint calibration of runoff generation and concentration parameters. While a calibratable mechanism may underperform a fixed-parameter setup in isolation, it offers greater flexibility. When jointly calibrated with runoff generation parameters, its performance can surpass that of the fixed-parameter mechanism (as in Table 6). The importance of

600 joint (i.e., hydrological and routing) parameter search strategies has also been emphasized in previous research (Cortés-Salazar et al., 2023). Second, the grid-level RVIC spatial parameterization scheme based on predefined transfer functions demonstrates a clear advantage, despite incorporating only minimal river network information (i.e., accumulation area and flow distance). To test for robustness, the experiment was repeated using the runoff generation parameters of the most complex Case 4; this repetition confirmed the consistency of the findings (Table S1).

605

For a more detailed analysis of the inter-case differences, a comparison of their streamflow simulation residuals was conducted (Fig. 14). The first observation is that the residual scatter points for Cases 2 and 3 cluster around the 1:1 line, indicating no significant difference in their simulation residuals. This suggests that, by default, using the officially recommended RVIC values is a viable approach. In contrast, a comparison between Case 2 and Case 4 reveals a clear

610 difference. Case 4 demonstrates reduced underestimation of high flows (Quadrant III), suggesting better peak performance, at the cost of overestimating medium and low flows (Quadrant I). This behaviour is more pronounced at the Shiquan outlet

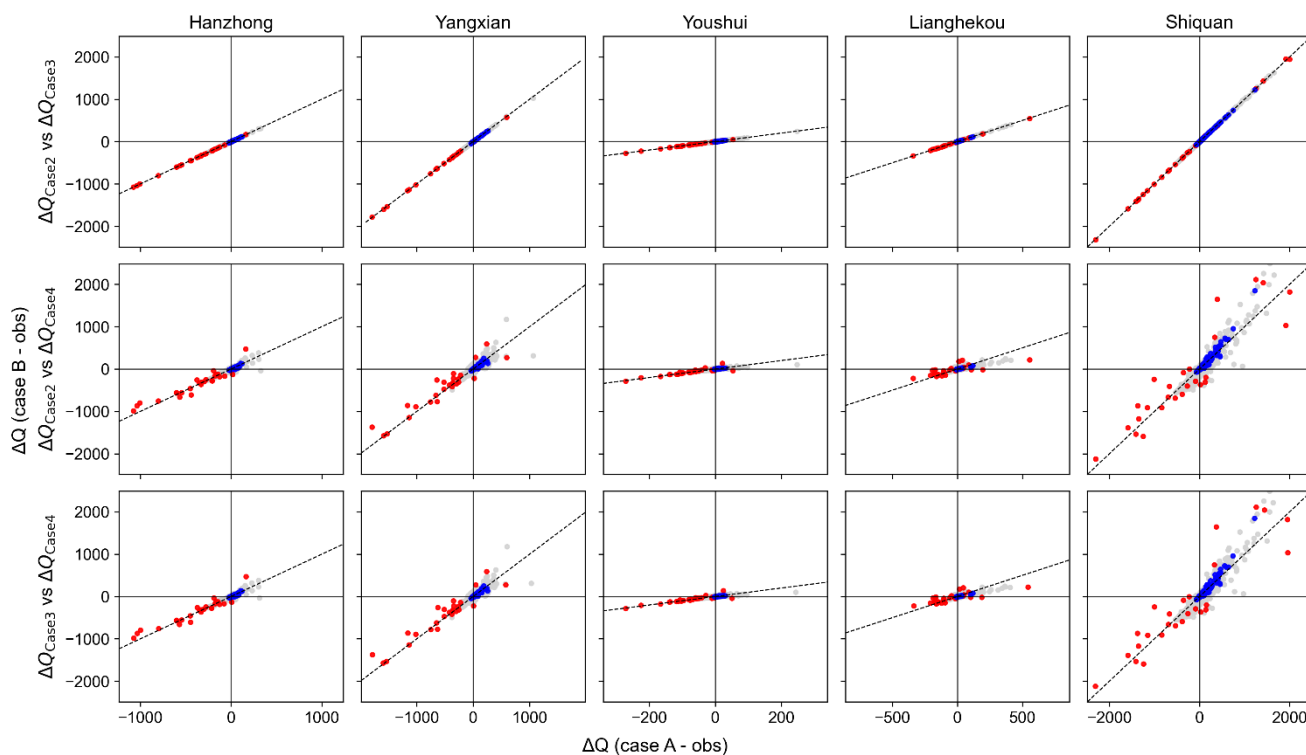


station. Likewise, the robustness of these findings was further confirmed through a repeated experiment based on the runoff generation parameters of Case 4, as shown in Fig. S3.

615 In many previous hydrological modelling applications, researchers have often focused considerable effort on improving the representation and calibration of runoff generation processes (Wang et al., 2022), while seemingly paying less attention to runoff concentration mechanisms. However, the findings of this study suggest that even minimal refinements to the spatial parametrization of the RVIC model—such as those implemented here—can lead to significant improvements in streamflow simulation, particularly for peak flows which are of critical concern. It should be acknowledged that the transfer functions  
620 employed in this study are relatively simple, incorporating only limited river network information (i.e., accumulation area and flow distance). Future work could therefore explore more sophisticated parametrizations in this direction, for example, by integrating hydraulic characteristics such as channel geometry and roughness into the transfer function, or by developing regionalized transfer functions based on machine learning techniques (Kupzig et al., 2024; Askarzadeh Farahani et al., 2025; Mohammed Ali et al., 2025). A meaningful insight emerging from this work for the development of next-generation  
625 distributed hydrological models is that advances in model parametrization should be pursued in tandem with calibration strategies that explicitly account for the resulting changes in parameter identifiability. This consideration applies equally to future developments that seek to enhance the complexity of runoff routing mechanisms.

**Table 10. Performance comparison of Cases 3, 2, and 4 during the validation period, with runoff generation parameters held constant as in Case 3. Performance is quantified by the KGE metrics, with the best value for each sub-basin shown in bold.**

	Hanzhong	Yangxian	Youshui	Lianghekou	Shiquan
Case 3	0.518	0.605	0.379	0.608	0.678
Case 2	0.516	0.605	0.372	0.600	0.677
Case 4	<b>0.534</b>	<b>0.646</b>	<b>0.450</b>	<b>0.726</b>	<b>0.682</b>



630

**Figure 14.** Scatter plots of simulated streamflow residuals ( $\Delta Q$ ) for Cases 3, 2, and 4 during the validation period, using the runoff generation parameters from Case 3. Red and blue dots represent high flows (exceedance probability < 2%) and low flows (exceedance probability > 70%), respectively. The dashed line indicates the 1:1 line.

## 5 Conclusion

635 Advances in measurement technique and computational capacity are accelerating the shift in hydrological modelling toward Model–Data Infusion framework. Along this line of development, the need to adopt spatially explicit parameterizations and implement stronger calibration constraints for improved model realism is widely acknowledged in the scientific community. However, current understanding of the integrated efficacy associated with these two approaches remains insufficient, particularly within the context of highly complex modern distributed hydrological models. By integrating the multiscale parameter regionalization technique with the Variable Infiltration Capacity model, this study develops an Experiment Framework to evaluate the effect of Spatially explicit Parameterization and Multi-gauge calibration, termed EF-SPM. The framework is then applied to conduct a series of comparative calibration experiments in a representative nested catchment, comprising eight cases with different parameterization and calibration configurations, with the aim of examining the synergies between these two aspects.

645



On the basis of the results from seven experiments within the EF-SPM, all configurations achieved satisfactory performance, as indicated by KGE values exceeding 0.76 during calibration and 0.67 during validation. Among them, more complex spatially explicit parameterization combined with stronger multi-gauge constraint consistently led to enhanced performance across all sub-basins. Considering the individual effects, spatially explicit parameterization exerted a compound influence on the simulations across multiple dimensions, including outlet hydrographs, runoff partitioning, and spatial distributions. It improved the simulation of moderate-flow to high-flow conditions at all gauges and substantially enhanced peak flows, indicated by  $\%Bias_{FHV_1}$  performing 18% better at the main outlet; however, low-flow performance deteriorated, with  $\%Bias_{FLV}$  performing 8.6% worse. The multi-gauge calibration strategy offers a distinct advantage over its single-gauge counterpart by significantly enhancing parameter identifiability, demonstrated in the more clustered distribution of optimal and sampled candidate solutions within the parameter space. From this perspective, a potential risk associated with spatially explicit parameterization is a reduction in identifiability, which implies an increase in equifinality.

Importantly, this study reveals a cross-benefit between spatially explicit parameterization and multi-gauge calibration. Comparison of scatter plot matrices in the multidimensional objective space reveals that, under uniform parameterization, pronounced trade-offs exist among the objectives of multiple gauges, forming continuous and convex arc-shaped Pareto fronts that severely constrain further improvement of model performance. This limitation is markedly alleviated under spatially explicit parameterization refinement. Collectively, our findings suggest that enhancements in spatial representation and the strengthening of calibration constraints should be pursued in parallel during the model development. Focusing on either aspect in isolation is unlikely to produce genuinely reliable improvements and may result in right results for the wrong reasons. As a further exploration, we demonstrate the effectiveness of the additional VIC-specific refinements introduced to the MPR in this study. These include the discretization of soil layer depths at the sub-basin scale and the spatialization mechanism for RVIC parameters at the grid scale. While relatively simple, these refinements delineate a viable pathway for advancing distributed hydrological models and regionalization approaches, which could be further explored in future work.



### Code availability

670 The documentation of Easy VIC Build (EVB) is provided at [https://xudongzhengsteven.github.io/easy\\_vic\\_build/](https://xudongzhengsteven.github.io/easy_vic_build/) (last  
access: 28 November 2025). The code used in this study is available through Zenodo via  
<https://doi.org/10.5281/zenodo.18076164> (Zheng, 2025).

### Data availability

All data used in this study is freely available through public open-source platforms, with the exception of streamflow  
675 observations, which were obtained from the China Hydrological Yearbooks. The CMFD is provided by National Tibetan  
Plateau / Third Pole Environment Data Center (<http://data.tpdac.ac.cn>). The SoilGrids1km dataset is publicly available from  
the official website: <https://soilgrids.org> (Poggio et al., 2021). Topographic data were derived from the STRM DEM dataset  
(Jarvis et al., 2008), available at <http://srtm.csi.cgiar.org/srtmdata/>, and land cover information was obtained from the UMD  
Land Cover product (Hansen et al., 2021), accessible at <https://iridl.ldeo.columbia.edu/SOURCES/UMD/GLCF/GLCDS/>.  
680 Remote sensing data from MODIS, including MCD43D51.061 BSA (Schaaf and Wang, 2021), MOD13A3.061 NDVI  
(Didan, 2021), and MOD15A2H.061 LAI (Myneni et al., 2021), were downloaded from the Land Processes Distributed  
Active Archive Center (LP DAAC) (<https://lpdaac.usgs.gov/>). Additionally, soil temperature data were obtained from the  
ERA5 Land dataset (Muñoz Sabater, 2019), available at [https://cds.climate.copernicus.eu/datasets/reanalysis-era5-land-  
monthly-means](https://cds.climate.copernicus.eu/datasets/reanalysis-era5-land-monthly-means). All datasets were accessed between September 2024 and December 2025 and are freely available for  
685 research purposes. We sincerely thank the data providers for their valuable contributions and for providing open access to  
these datasets.

### Author contributions

XDZ was responsible for conceptualization, data curation, formal analysis, and writing – original draft. DFL contributed to  
conceptualization, supervision, writing – review & editing, and funding acquisition. HW provided supervision. CHM  
690 provided resources. HL and GHM participated in conceptualization. QL, MYAK, and FH assisted with writing – review &  
editing.

### Competing interests

The authors declare that they have no conflict of interest.



### **Acknowledgements**

695 This work was performed as part of the PhD project of Xudong Zheng.

### **Financial support**

This study was financially supported by the National Natural Science Foundation of China (Grant No. 52279025) and the National Key R&D Program of China (2022YFF1302200).



## References

- 700 Aerts, J., Hut, R., van de Giesen, N., Drost, N., Verseveld, W., Weerts, A., and Hazenberg, P.: Large-sample assessment of varying spatial resolution on the streamflow estimates of the wflow\_sbm hydrological model, *Hydrology and Earth System Sciences*, 26, 4407-4430, 10.5194/hess-26-4407-2022, 2022.
- Aerts, Jerom P. M., Hoch, Jannis M., Coxon, G., van de Giesen, Nick C., and Hut, Rolf W.: On the importance of discharge observation uncertainty when interpreting hydrological model performance, *Hydrology and Earth System Sciences*, 28, 5011-5030, 10.5194/hess-28-5011-2024, 2024.
- 705 Argentin, A. L., Horton, P., Schaefli, B., Shokory, J., Pitscheider, F., Repnik, L., Gianini, M., Bizzi, S., Lane, S. N., and Comiti, F.: Scale dependency in modeling nivo-glacial hydrological systems: the case of the Arolla basin, Switzerland, *Hydrol. Earth Syst. Sci.*, 29, 1725-1748, 10.5194/hess-29-1725-2025, 2025.
- Askarzadeh Farahani, M., Wood, A., Tang, G., and Mizukami, N.: Calibrating a large-domain land/hydrology process model in the age of AI: the SUMMA CAMELS emulator experiments, *Hydrology and Earth System Sciences*, 29, 4515-4537, 10.5194/hess-29-4515-2025, 2025.
- 710 Balsamo, G., Viterbo, P., Beljaars, A., Hurk, B., Hirschi, M., Betts, A., and Scipal, K.: A Revised Hydrology for the ECMWF Model: Verification from Field Site to Terrestrial Water Storage and Impact in the Integrated Forecast System, *Journal of Hydrometeorology*, 10, 623, 10.1175/2008JHM1068.1, 2009.
- 715 Beven, K.: How Far Can We Go in Distributed Hydrological Modeling, *Hydrology and Earth System Sciences*, 5, 10.5194/hess-5-1-2001, 2001.
- Beven, K.: A brief history of information and disinformation in hydrological data and the impact on the evaluation of hydrological models, *Hydrological Sciences Journal*, 69, 519-527, 10.1080/02626667.2024.2332616, 2024.
- Bohn, T. J. and Vivoni, E. R.: MOD-LSP, MODIS-based parameters for hydrologic modeling of North American land cover change, *Scientific Data*, 6, ARTN 14410.1038/s41597-019-0150-2, 2019.
- 720 Brunner, M. I., Melsen, L. A., Wood, A. W., Rakovec, O., Mizukami, N., Knoben, W. J. M., and Clark, M. P.: Flood spatial coherence, triggers, and performance in hydrological simulations: large-sample evaluation of four streamflow-calibrated models, *Hydrology and Earth System Sciences*, 25, 105-119, 10.5194/hess-25-105-2021, 2021.
- Casper, M., Grigoryan, G., Gronz, O., Gutjahr, O., Heinemann, G., Ley, R., and Rock, A.: Analysis of projected hydrological behavior of catchments based on signature indices, *Hydrology and Earth System Sciences*, 16, 409-421, 10.5194/hess-16-409-2012, 2012.
- 725 Chagas, V., Chaffe, P., and Blöschl, G.: Regional Low Flow Hydrology: Model Development and Evaluation, *Water Resources Research*, 60, 10.1029/2023WR035063, 2024.
- Chen, Y., Shi, P., Ji, X., Qu, S., Zhao, L., and Dong, F.: New method to calculate the dynamic factor–flow velocity in Geomorphologic instantaneous unit hydrograph, *Scientific Reports*, 9, 10.1038/s41598-019-50723-x, 2019.
- 730



- Clark, M., Lamontagne, J., Mizukami, N., Knoben, W., Tang, G., Gharari, S., Freer, J., Whitfield, P., Shook, K., and Papalexiou, S. M.: The Abuse of Popular Performance Metrics in Hydrologic Modeling, *Water Resources Research*, 57, 10.1029/2020WR029001, 2021.
- 735 Clark, M., Nijssen, B., Lundquist, J., Kavetski, D., Rupp, D., Woods, R., Freer, J., Gutmann, E., Wood, A., Brekke, L., Arnold, J., Gochis, D., and Rasmussen, R.: A unified approach for process-based hydrologic modeling: 1. Modeling concept, *Water Resources Research*, 51, 10.1002/2015WR017198, 2015.
- Cortés-Salazar, N., Vasquez, N., Mizukami, N., Mendoza, P., and Vargas, X.: To what extent does river routing matter in hydrological modeling?, *Hydrology and Earth System Sciences*, 27, 3505-3524, 10.5194/hess-27-3505-2023, 2023.
- 740 Cosby Jr, B., Hornberger, G., Clapp, R., and Ginn, T.: A Statistical Exploration of Relationships of Soil Moisture Characteristics to the Physical Properties of Soils, *Water Resources Research - WATER RESOUR RES*, 20, 682-690, 10.1029/WR020i006p00682, 1984.
- De Rainville, F.-M., Fortin, F.-A., Gardner, M.-A., Parizeau, M., and Gagné, C.: DEAP: A Python framework for Evolutionary Algorithms, 85-92 pp., 10.1145/2330784.2330799, 2012.
- 745 Didan, K.: MODIS/Terra Vegetation Indices Monthly L3 Global 1km SIN Grid V061 (V061) [dataset], 10.5067/MODIS/MOD13A3.061, 2021.
- Duc, N., Oki, T., and Kanae, S.: A variable streamflow velocity method for global river routing model: Model description and preliminary results, *Hydrology and Earth System Sciences Discussions*, 4, 10.5194/hessd-4-4389-2007, 2007.
- Dumenil, L. and Todini, E.: A rainfall-runoff scheme for use in the Hamburg climate model, *Advances in theoretical hydrology*, 129-157, 1992.
- 750 Feng, D., Liu, J., Lawson, K., and Shen, C.: Differentiable, Learnable, Regionalized Process-Based Models With Multiphysical Outputs can Approach State-Of-The-Art Hydrologic Prediction Accuracy, *Water Resources Research*, 58, 10.1029/2022WR032404, 2022.
- Fenicia, F. and Kavetski, D.: Behind every robust result is a robust method: Perspectives from a case study and publication process in hydrological modelling, *Hydrol Process*, 35, 2021.
- 755 Fortin, F.-A., De Rainville, F.-M., Gardner, M. A., Parizeau, M., and Gagné, C.: DEAP: Evolutionary algorithms made easy, *Journal of Machine Learning Research*, *Machine Learning Open Source Software*, 13, 2171-2175, 2012.
- Freeze, R. A. and Harlan, R. L.: Blueprint for a physically-based, digitally-simulated hydrologic response model, *Journal of Hydrology*, 9, 237-258, 10.1016/0022-1694(69)90020-1, 1969.
- 760 Gou, J., Miao, C., Duan, Q., Tang, Q., di, Z., Liao, W., Wu, J., and Zhou, R.: Sensitivity analysis-based automatic parameter calibration of the variable infiltration capacity (VIC) model for streamflow simulations over China, *Water Resources Research*, 56, 10.1029/2019WR025968, 2020.
- Guo, J.: General and Analytic Unit Hydrograph and Its Applications, *Journal of Hydrologic Engineering*, 27, 10.1061/(ASCE)HE.1943-5584.0002149, 2022.



- 765 Gupta, H., Sorooshian, S., and Yapo, P.: Toward improved calibration of hydrologic models: Multiple and noncommensurable measures of information, *Water Resources Research - WATER RESOUR RES*, 34, 10.1029/97WR03495, 1998.
- Gupta, H., Wagener, T., and Liu, Y.: Reconciling Theory with Observations: Elements of a Diagnostic Approach to Model Evaluation, *Hydrol Process*, 22, 3802-3813, 10.1002/hyp.6989, 2008.
- 770 Gupta, H., Perrin, C., Blöschl, G., Montanari, A., Kumar, R., Clark, M., and Andréassian, V.: Large-sample hydrology: a need to balance depth with breadth, *Hydrology and Earth System Sciences*, 18, 10.5194/hess-18-463-2014, 2014.
- Guse, B., Han, L., Kumar, R., Rakovec, O., Luedtke, S., Herzog, A., Thober, S., Samaniego, L., and Wagener, T.: Spatio-Temporal Consistency and Variability in Parameter Dominance on Simulated Hydrological Fluxes and State Variables, *Water Resources Research*, 60, 10.1029/2023WR036822, 2024.
- 775 Hamman, J. J., Nijssen, B., Bohn, T. J., Gergel, D. R., and Mao, Y. X.: The Variable Infiltration Capacity model version 5 (VIC-5): infrastructure improvements for new applications and reproducibility, *Geosci Model Dev*, 11, 3481-3496, 10.5194/gmd-11-3481-2018, 2018.
- Hansen, M., Defries, R., Townshend, J., and Sohlberg, R.: Global land cover classification at 1km resolution using a decision tree classifier, *J Remote Sens*, 2021.
- Hansen, N. and Ostermeier, A.: Completely Derandomized Self-Adaptation in Evolution Strategies, *Evolutionary*  
780 *Computation*, 9, 159-195, 10.1162/106365601750190398, 2001.
- He, J.: China Meteorological Forcing Dataset - 03-hourly (Version 1) [dataset], <https://doi.org/10.6084/m9.figshare.9200753.v1>, 2020.
- He, J., Yang, K., Tang, W., Lu, H., Qin, J., Chen, Y., and Li, X.: The first high-resolution meteorological forcing dataset for land process studies over China, *Sci Data*, 7, 25, 10.1038/s41597-020-0369-y, 2020.
- 785 Hengl, T., Mendes de Jesus, J., Macmillan, R. A., Batjes, N., Heuvelink, G., Ribeiro, E., Samuel-Rosa, A., Kempen, B., Leenaars, J. G. B., Walsh, M., and Gonzalez, M.: SoilGrids1km — Global Soil Information Based on Automated Mapping, *Plos One*, 9, e105992, 10.1371/journal.pone.0105992, 2014.
- Heuer, M. M., Mohajerani, H., and Casper, M. C.: Multi-variable process-based calibration of a behavioural hydrological model, *EGUsphere*, 2025, 1-41, 10.5194/egusphere-2025-636, 2025.
- 790 Hurk, B. and Viterbo, P.: The Torne-Kalix PILPS 2(e) experiment as a test bed for modifications to the ECMWF land surface scheme, *Global Planet Change*, 38, 165-173, 10.1016/S0921-8181(03)00027-4, 2003.
- J S, N. and Mishra, V.: Multiday Precipitation Is a Prominent Driver of Floods in Indian River Basins, *Water Resources Research*, 58, 10.1029/2022WR032723, 2022.
- 795 Jarvis, A., Reuter, H., Nelson, A., and Guevara, E.: Hole-filled seamless SRTM data V4. Tech. rep., International Centre for Tropical Agriculture (CIAT), Cali, Columbia, 2008.
- K, S., M, H., and Doell, P.: Simulating river flow velocity on global scale, *Advances in Geosciences*, 5, 10.5194/adgeo-5-133-2005, 2005.



- 800 Kholis, A., Kalbacher, T., Rakovec, O., Boeing, F., Cuntz, M., and Samaniego, L.: Evaluating Richards Equation and Infiltration Capacity Approaches in Mesoscale Hydrologic Modeling, *Water Resources Research*, 61, 10.1029/2024WR039625, 2025.
- Kittel, C. M. M., Nielsen, K., Tottrup, C., and Bauer-Gottwein, P.: Informing a hydrological model of the Ogooue with multi-mission remote sensing data, *Hydrology and Earth System Sciences*, 22, 1453-1472, 2018.
- Knoben, W., Freer, J., Peel, M., Fowler, K., and Woods, R.: A Brief Analysis of Conceptual Model Structure Uncertainty Using 36 Models and 559 Catchments, *Water Resources Research*, 56, e2019WR025975, 10.1029/2019WR025975, 805 2020.
- Kupzig, J., Kupzig, N., and Flörke, M.: Regionalization in global hydrological models and its impact on runoff simulations: a case study using WaterGAP3 (v 1.0.0), *Geosci Model Dev*, 17, 6819-6846, 10.5194/gmd-17-6819-2024, 2024.
- Lehmann, F., Vishwakarma, B., and Bamber, J.: How well are we able to close the water budget at the global scale?, *Hydrology and Earth System Sciences*, 26, 35-54, 10.5194/hess-26-35-2022, 2022.
- 810 Li, T., Liu, D., Han, S., Ming, G., Fan, J., Meng, X., and Huang, Q.: Closing the Feedback of Evapotranspiration on the Atmospheric Evaporation Demand Based on a Complementary Relationship, *Atmosphere*, 13, 10.3390/atmos13091431, 2022.
- Li, X., Liu, F., Ma, C., Hou, J., Zheng, D., Hanqing, M., Bai, Y., Han, X., Vereecken, H., Yang, K., Duan, Q., and Huang, C.: Land Data Assimilation: Harmonizing Theory and Data in Land Surface Process Studies, *Reviews of Geophysics*, 62, 815 10.1029/2022RG000801, 2024.
- Liang, X. and Xie, Z.: A new surface runoff parameterization with subgrid-scale soil heterogeneity for land surface model, *Adv Water Resour*, 24, 1173-1193, 10.1016/S0309-1708(01)00032-X, 2001.
- Liang, X., Lettenmaier, D. P., Wood, E., and Burges, S.: A simple hydrologically based model of land-surface water and energy fluxes for general-circulation models, *J. Geophys. Res.*, 99, 14415-14428, 10.1029/94JD00483, 1994.
- 820 Lin, Q., Wu, Z., Liu, J., Singh, V., and Zuo, Z.: Hydrological drought dynamics and its teleconnections with large-scale climate indices in the Xijiang River basin, South China, *Theoretical and Applied Climatology*, 10.1007/s00704-022-04153-x, 2022.
- Liu, P., Liu, D., Khan, M. Y. A., Zheng, X., Hu, Y., Ming, G., and Gao, M.: Multivariate Validation at Multistation of Distributed Watershed Hydrological Modeling Based on Multisource Data on Chinese Loess Plateau, *Water*, 16, 1823, 825 2024.
- Liu, Y., Weerts, A., Clark, M., Franssen, H.-J., Kumar, S., Hamid, M., Seo, D.-J., Schwanenberg, D., Smith, P., van Dijk, A., Velzen, N., He, M., Lee, H., Noh, S. J., Rakovec, O., and Restrepo, P.: Advancing data assimilation in operational hydrologic forecasting: Progresses, challenges, and emerging opportunities, *Hydrology and Earth System Sciences*, 16, 10.5194/hess-16-3863-2012, 2012.



- 830 Lohmann, D., Nolte-Holube, R., and Raschke, E.: A large-scale horizontal routing model to be coupled to land surface parametrization schemes, *Tellus, Series A: Dynamic Meteorology and Oceanography*, 48, 708-721, 10.3402/tellusa.v48i5.12200, 1996.
- Luo, Z. and Shao, Q.: A modified hydrologic model for examining the capability of global gridded PET products in improving hydrological simulation accuracy of surface runoff, streamflow and baseflow, *Journal of Hydrology*, 610, 127960, 10.1016/j.jhydrol.2022.127960, 2022.
- 835 Ma, L., Liu, D., Luan, J., Guanghui, M., Meng, X., and Huang, Q.: Connecting flow duration curve and precipitation duration curve based on the relationship deduced from machine learning in the watersheds of northern China, *Journal of Hydrology*, 635, 131235, 10.1016/j.jhydrol.2024.131235, 2024.
- Mei, Y., Mai, J., Do, H., Gronewold, A., Reeves, H., Eberts, S., Niswonger, R., Regan, R., and Hunt, R.: Can Hydrological Models Benefit From Using Global Soil Moisture, Evapotranspiration, and Runoff Products as Calibration Targets?, *Water Resources Research*, 59, 10.1029/2022WR032064, 2023.
- 840 Melsen, L., Teuling, A., Torfs, P., Zappa, M., Mizukami, N., Clark, M., and Uijlenhoet, R.: Representation of spatial and temporal variability in large-domain hydrological models: case study for a mesoscale pre-Alpine basin, *Hydrology and Earth System Sciences*, 20, 2207-2226, 10.5194/hess-20-2207-2016, 2016.
- 845 Mizukami, N., Clark, M., Newman, A., Wood, A., Gutmann, E., Nijssen, B., Rakovec, O., and Samaniego, L.: Toward seamless large domain parameter estimation for hydrologic models, *Water Resources Research*, 53, 10.1002/2017wr020401, 2017.
- Mohammed Ali, A., Imhoff, R., and Weerts, A.: Machine Learning for Predicting Spatially Variable Lateral Hydraulic Conductivity: A Step Toward Efficient Hydrological Model Calibration and Global Applicability, *Water Resources Research*, 61, 10.1029/2025WR040108, 2025.
- 850 Muñoz Sabater, J., Dutra, E., Agusti-Panareda, A., Albergel, C., Arduini, G., Balsamo, G., Boussetta, S., Choulga, M., Harrigan, S., Hersbach, H., Martens, B., Miralles, D., Piles, M., Rodriguez-Fernandez, N., Zsótér, E., Buontempo, C., and Thépaut, J. N.: ERA5-Land: A state-of-the-art global reanalysis dataset for land applications, *Earth System Science Data*, 13, 4349-4383, 10.5194/essd-13-4349-2021, 2021.
- 855 Myneni, R., Knyazikhin, Y., and Park, T.: MODIS/Terra Leaf Area Index/FPAR 8-Day L4 Global 500m SIN Grid V061 (V061) [dataset], 10.5067/MODIS/MOD15A2H.061, 2021.
- Nasta, P., Blöschl, G., Bogen, H., Zacharias, S., Baatz, R., De Lannoy, G., Jensen, K., Manfreda, S., Pfister, L., Tarquis Alfonso, A., van Meerveld, I., Voltz, M., Zeng, Y., Kustas, W., Li, X., Vereecken, H., and Romano, N.: HESS Opinions: Towards a common vision for the future of hydrological observatories, *Hydrology and Earth System Sciences*, 29, 465-483, 10.5194/hess-29-465-2025, 2025.
- 860 Nijssen, B., Lettenmaier, D., Lohmann, D., and Wood, E.: Predicting the Discharge of Global Rivers, *Journal of Climate - J CLIMATE*, 14, 3307-3323, 10.1175/1520-0442(2001)014<3307:PTDOGR>2.0.CO;2, 2001.



- Poggio, L., Batjes, N., Heuvelink, G., Kempen, B., Ribeiro, E., and Rossiter, D.: SoilGrids 2.0: producing soil information for the globe with quantified spatial uncertainty, *Soil-Germany*, 7, 217-240, 10.5194/soil-7-217-2021, 2021.
- 865 Pool, S., Fowler, K., Gardiya Weligamage, H., and Peel, M.: Multivariate calibration can increase simulated discharge uncertainty and model equifinality, *EGUsphere*, 2025, 1-26, 10.5194/egusphere-2025-1598, 2025.
- Roy, A. and Thomas, R.: A Comparative Study on the Derivation of Unit Hydrograph for Bharathapuzha River Basin, *Procedia Technology*, 24, 62-69, 10.1016/j.protcy.2016.05.010, 2016.
- Samaniego, L., Kumar, R., and Attinger, S.: Multiscale parameter regionalization of a grid-based hydrologic model at the mesoscale, *Water Resour. Res.*, 46, 10.1029/2008WR007327, 2010.
- 870 Schaaf, C. and Wang, Z.: MODIS/Terra+Aqua BRDF/Albedo Black Sky Albedo Shortwave Daily L3 Global 30ArcSec CMG V061 (V061) [dataset], 10.5067/MODIS/MCD43D51.061, 2021.
- Shrestha, R., Cannon, A., Hoffman, S., Whibley, M., and Lima, A.: Benchmarking historical performance and future projections from a large-scale hydrologic model with a watershed hydrologic model, *Hydrology and Earth System Sciences*, 29, 2881-2900, 10.5194/hess-29-2881-2025, 2025.
- 875 Sun, R., Pan, B., and Duan, Q.: A surrogate modeling method for distributed land surface hydrological models based on deep learning, *Journal of Hydrology*, 624, 129944, 10.1016/j.jhydrol.2023.129944, 2023.
- Sun, R., Pan, B., and Duan, Q.: Learning Distributed Parameters of Land Surface Hydrologic Models Using a Generative Adversarial Network, *Water Resources Research*, 60, 10.1029/2024WR037380, 2024.
- 880 Sun, Y., Tian, F., Yang, L., and Hu, H.: Exploring the spatial variability of contributions from climate variation and change in catchment properties to streamflow decrease in a mesoscale basin by three different methods, *Journal of Hydrology*, 508, 10.1016/j.jhydrol.2013.11.004, 2013.
- Széles, B., Parajka, J., Hogan, P., Silasari, R., Pavlin, L., Strauss, P., and Blöschl, G.: The Added Value of Different Data Types for Calibrating and Testing a Hydrologic Model in a Small Catchment, *Water resources research*, 56, 885 e2019WR026153, 10.1029/2019WR026153, 2020.
- Talbot, F., Sylvain, J. D., Drolet, G., Poulin, A., and Arsenault, R.: Enhancing physically based and distributed hydrological model calibration through internal state variable constraints, *Hydrol. Earth Syst. Sci.*, 29, 6549-6576, 10.5194/hess-29-6549-2025, 2025.
- Thober, S., Müller, S., Kelbling, M., Kumar, R., Attinger, S., and Samaniego, L.: MPR 1.0: a stand-alone multiscale parameter regionalization tool for improved parameter estimation of land surface models, *Geosci Model Dev*, 15, 859-882, 10.5194/gmd-15-859-2022, 2022.
- 890 Tudaji, M., Nan, Y., and Tian, F.: Assessing the value of high-resolution rainfall and streamflow data for hydrological modeling: an analysis based on 63 catchments in southeast China, *Hydrol. Earth Syst. Sci.*, 29, 1919-1937, 10.5194/hess-29-1919-2025, 2025.
- 895 Wambura, F. J., Dietrich, O., and Lischeid, G.: Improving a distributed hydrological model using evapotranspiration-related boundary conditions as additional constraints in a data-scarce river basin, *Hydrol Process*, 32, 759-775, 2018.



- Wang, Z., Tang, Q., Wang, D., Xiao, P., Xia, R., Sun, P., and Feng, F.: Attributing trend in naturalized streamflow to temporally explicit vegetation change and climate variation in the Yellow River basin of China, *Hydrol. Earth Syst. Sci.*, 26, 5291-5314, 10.5194/hess-26-5291-2022, 2022.
- 900 Wen, Z. Q., Liang, X., and Yang, S. T.: A new multiscale routing framework and its evaluation for land surface modeling applications, *Water Resources Research*, 48, Artn W0852810.1029/2011wr011337, 2012.
- Yang, Y., Endreny, T. A., and Nowak, D. J. J. o. E. s.: Application of advection-diffusion routing model to flood wave propagation: A case study on Big Piney River, Missouri USA, 27, 9-14, 2016.
- Yeste, P., García-Valdecasas Ojeda, M., Gámiz-Fortis, S. R., Castro-Díez, Y., Bronstert, A., and Esteban-Parra, M. J.: A  
905 large-sample modelling approach towards integrating streamflow and evaporation data for the Spanish catchments, *Hydrol. Earth Syst. Sci.*, 28, 5331-5352, 10.5194/hess-28-5331-2024, 2024.
- Yilmaz, K., Gupta, H., and Wagener, T.: A process-based diagnostic approach to model evaluation: Application to the NWS distributed hydrologic model, *Water Resources Research - WATER RESOUR RES*, 44, 10.1029/2007WR006716, 2008.
- Yousefi Sohi, H., Zahraie, B., Dolatabadi, N., and Zebarjadian, F.: Application of VIC-WUR model for assessing the  
910 spatiotemporal distribution of water availability in anthropogenically-impacted basins, *Journal of Hydrology*, 637, 131365, 10.1016/j.jhydrol.2024.131365, 2024.
- Zhao, X., Liu, D., Wei, X., Ma, L., Lin, M., Meng, X., and Huang, Q.: Analysis of Socio-Hydrological Evolution Processes Based on a Modeling Approach in the Upper Reaches of the Han River in China, *Water*, 13, 10.3390/w13182458, 2021.
- Zheng, X., Liu, D., Huang, S., Wang, H., and Meng, X.: Achieving water budget closure through physical hydrological  
915 process modelling: insights from a large-sample study, *Hydrol. Earth Syst. Sci.*, 29, 627-653, 10.5194/hess-29-627-2025, 2025.
- Zheng, X. (2025). Code for the paper "What can Hydrological Modelling gain from Spatially Explicit Parameterization and Multi-gauge Calibration?". Zenodo. <https://doi.org/10.5281/zenodo.18076164>.